Differential requirement of kindlin-3 for T cell progenitor homing to the non-vascularized and vascularized thymus

Federico Andrea Moretti[1†], Sarah Klapproth[1†], Raphael Ruppert[1], Andreas Margraf[2], Jasmin Weber[2], Robert Pick[2], Christoph Scheiermann[2], Markus Sperandio[2], Reinhard Fässler[1], Markus Moser[1*]

[1]Department Molecular Medicine, Max-Planck-Institute of Biochemistry, Martinsried, Germany; [2]Walter Brendel Center of Experimental Medicine, Biomedical Center, Ludwig-Maximilians-Universität, Martinsried, Germany

Abstract The role of integrin-mediated adhesion during T cell progenitor homing to and differentiation within the thymus is ill-defined, mainly due to functional overlap. To circumvent compensation, we disrupted the hematopoietic integrin regulator kindlin-3 in mice and found a progressive thymus atrophy that is primarily caused by an impaired homing capacity of T cell progenitors to the vascularized thymus. Notably, the low shear flow conditions in the vascular system at midgestation allow kindlin-3-deficient fetal liver-derived T cell progenitors to extravasate via pharyngeal vessels and colonize the avascular thymus primordium. Once in the thymus, kindlin-3 promotes intrathymic T cell proliferation by facilitating the integrin-dependent crosstalk with thymic antigen presenting cells, while intrathymic T cell migration, maturation into single positive CD4 and CD8 T cells and release into the circulation proceed without kindlin-3. Thus, kindlin-3 is dispensable for integrin-mediated T cell progenitor adhesion and signalling at low and indispensable at high shear forces.

DOI: https://doi.org/10.7554/eLife.35816.001

*For correspondence:
moser@biochem.mpg.de

†These authors contributed equally to this work

Introduction

T cell progenitors develop in the fetal liver (FL) or in the bone marrow (BM) and require the specialized environment of the thymus to mature into single positive (SP) CD4 or CD8 T cells (*Cai et al., 2007*; *Foss et al., 2001*; *Jotereau et al., 1987*). FL-derived T cell progenitors start colonizing the thymus anlage at around embryonic day (E) 11.5. Since the thymus anlage is initially avascular, T cell progenitors exit the adjacent pharyngeal vessels, migrate towards the thymic primordium, cross the dense extracellular matrix of the thymic capsule and finally settle in the thymic tissue. After thymus vascularization, which occurs at around E15 (*Liu et al., 2006*), T cell progenitors enter the thymus by extravasating from post-capillary venules at the cortico-medullary junction. Once in the thymus the progenitor cells interact and receive signals from thymic epithelial cells, macrophages, dendritic cells (DCs) and extracellular matrix proteins, which are essential for their proliferation, differentiation, selection and release into the circulation as mature, single positive T cells (*Boehm and Bleul, 2006*; *Koch and Radtke, 2011*).

Leukocyte extravasation follows a cascade of adhesion events commencing with selectin-mediated rolling of leukocytes on endothelial cells followed by the interaction with endothelial cell-bound chemokines, integrin-mediated leukocyte arrest and crawling and finally the transmigration through the vessel wall (*Ley et al., 2007*). Although integrins are expressed on all hematopoietic cells, conflicting reports exist on their role for T cell progenitor extravasation. While the treatment with function-blocking antibodies against α4 and/or β2 integrins reduced the homing of thymic progenitors

to the adult thymus (*Rossi et al., 2005*; *Scimone et al., 2006*), genetic ablation of neither α4 (*Arroyo et al., 1996*), nor αL (*Schmits et al., 1996*), α6 (*Georges-Labouesse et al., 1996*), β2 (*Scharffetter-Kochanek et al., 1998*), β7 integrins (*Bungartz et al., 2006*; *Wagner et al., 1996*), or the integrin ligands intercellular adhesion molecule (ICAM)−1 and vascular cell adhesion molecule (VCAM)−1 (*Koni et al., 2001*; *Sligh et al., 1993*; *Xu et al., 1994*) interfered with thymic colonization. Similarly, it is not known whether migration of T cell progenitors within the thymus, or their proliferation and differentiation require integrin-mediated adhesion.

Kindlins are a family of β integrin tail binding proteins that regulate the affinity of integrins for their ligands and induce signal transduction pathways downstream of activated, ligand-bound integrins (*Moser et al., 2009b*). Kindlins consist of 3 members: kindlin-1,−2, and −3; while kindlin-1 and −2 are widely expressed, hematopoietic cells exclusively express kindlin-3 (*Ussar et al., 2006*; *Weinstein et al., 2003*). Consequently, loss of kindlin-3 impairs the functions of all integrins on hematopoietic cells studied so far and leads to severe defects affecting platelets, leukocytes, osteoclasts and hematopoietic stem and progenitor cells (HSPCs) (*Krüger et al., 2008*; *Moser et al., 2009a*; *Moser et al., 2008*; *Ruppert et al., 2015*; *Schmidt et al., 2011*). In line with genetic studies in mice, loss-of-function mutations in the human *KINDLIN-3/FERMT3* gene cause leukocyte adhesion deficiency type-III (LAD-III) syndrome, which is characterized by severe bleedings, infections and accumulation of HSPCs in the blood circulation (*Kuijpers et al., 2009*; *Malinin et al., 2009*; *Mory et al., 2008*; *Ruppert et al., 2015*; *Svensson et al., 2009*).

In the present study, we investigated T-lymphopoiesis in kindlin-3-deficient mice. We found that loss of kindlin-3 protein expression results in progressive thymus atrophy, which is mainly caused by impaired colonization of the vascularised thymus by BM-derived T cell progenitors during late embryogenesis and after birth. In contrast, however, colonization of the non-vascularized thymic primordium by kindlin-3-deficient FL-derived progenitors proceeded without kindlin-3, albeit less efficiently, due to the lower vascular shear flow in embryos. Within the thymus anlage, the proliferation rate of kindlin-3-deficient T cell populations was reduced, while differentiation into mature CD4 and CD8 T cells was unaffected. Thus, these findings clearly show the crucial role of integrins during T cell development. Specifically, in the absence of kindlin-3 only a weak integrin-mediated T cell adhesion can occur, which suffices resistance to low systemic shear forces and enables T cell progenitor homing early during development. However, at later time points during development, when vascular shear forces increase, kindlin-3 is critical to stabilize T cell adhesion on endothelial cells allowing T cell progenitor homing into the thymus.

Results

Loss of kindlin-3 protein leads to progressive thymus atrophy

Kindlin-3 is expressed in CD4/CD8 double negative (DN) and double positive (DP) T cells from wild-type (WT) thymi and SP CD4 and CD8 T cells from WT spleens (*Figure 1—figure supplement 1A*). To test whether kindlin-3 expression is required for thymopoiesis, we investigated thymus morphology and size in kindlin-3-deficient (*Fermt3⁻/⁻*) mice, which die of severe bleedings and anemia within the first week after birth (*Moser et al., 2008*). The morphology of *Fermt3⁻/⁻* thymi was normal and the size steadily increased until postnatal day (P) 3 (*Figure 1A,B*). However, while WT thymi continued to grow postnatally, *Fermt3⁻/⁻* thymi shrank and became atrophic (*Figure 1B*). Consistently, the cellularity of WT thymi continuously increased during development (*Figure 1C*), while *Fermt3⁻/⁻* thymi showed an increase in cellularity only until P3, followed by a dramatic decrease at P6 and P8 (*Figure 1C*). Despite the progressive increase in cellularity until P3 the number of cells was significantly lower in *Fermt3⁻/⁻* thymi compared to controls at all time points analyzed (*Figure 1C*). Importantly, we did not observe any compensatory expression of kindlin-1 or −2 in kindlin-3-deficient thymi (*Figure 1—figure supplement 1B*).

Hematoxylin/eosin (H/E) staining of thymic section at different stages of development revealed a similar formation of medullary islets in P0 WT and *Fermt3⁻/⁻* thymi that enlarged and fused at P3 to produce a large central medulla surrounded by the cortex (*Figure 1D*). In line with the normal thymic cyto-architecture at P3, *Fermt3⁻/⁻* thymi displayed normal cortico-medullary junctions (CMJ) that separate CD4/CD8 DP T cells in the cortex from SP CD4 and CD8 T cells in the medulla, and normal epithelial meshes and vascular networks (*Figure 1—figure supplement 1C*). At P6 and P8, however,
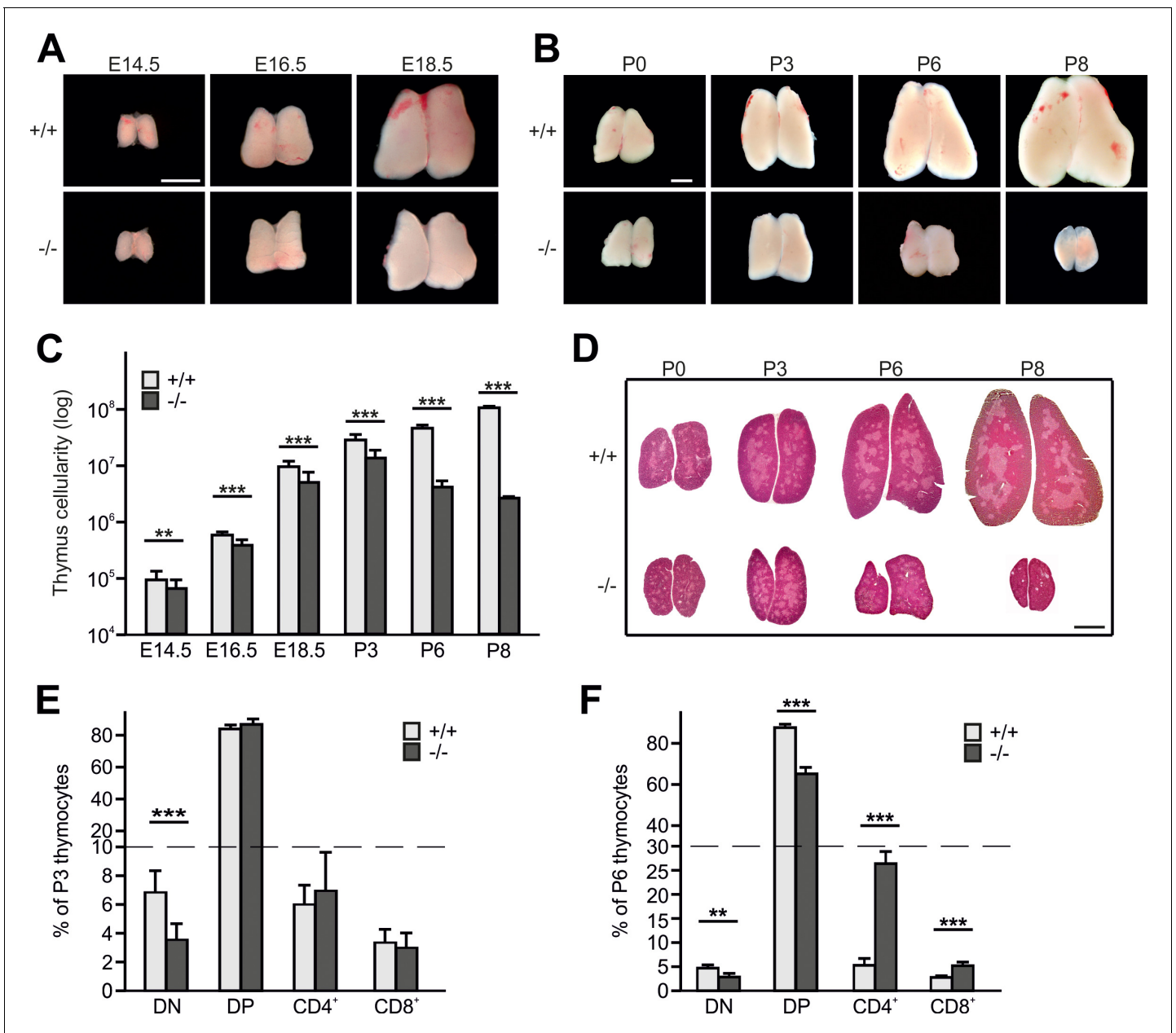
Figure 1. Kindlin-3 deficiency causes thymus atrophy. (A and B) Images from *Fermt3*^{+/+} (upper panel) and *Fermt3*^{-/-} (lower panel) thymi isolated at the indicated embryonic and postnatal stages. Scale bars 1 mm. (C) Total thymocyte numbers at indicated time points (E14.5 to P8). N(E14.5)=28/28; N (E16.5)=12/12; N(E18.5)=30/21; N(P3)=6/4; N(P8)=3/2. (D) Haematoxylin and Eosin staining of paraffin-embedded thymus sections. Scale bar 1 mm. (E and F) Frequencies of CD4 and CD8 double negative (DN), double positive (DP) and single positive CD4 and CD8 thymocytes isolated from P3 and P6 thymi. N(P3)=16/18; N(P6)=8/4. Bars indicate means ± standard errors. **p<0.01; ***p<0.001. See also *Figure 1—figure supplement 1*.

DOI: https://doi.org/10.7554/eLife.35816.002

The following figure supplement is available for figure 1:

Figure supplement 1. Kindlin-3 deficiency causes thymus atrophy.

DOI: https://doi.org/10.7554/eLife.35816.003

the atrophic *Fermt3*^{-/-} thymi showed a progressive enlargement of the medulla and a strong reduction of the cortex suggesting an imbalanced development towards more mature SP T cells (*Figure 1D*). This observation was confirmed by flow cytometry showing that DN T cells containing the most immature intrathymic T cells were significantly reduced at P3 and P6 in *Fermt3*^{-/-} thymi compared to controls. Notably, while the relative distribution of DP and SP CD4 and CD8 T cells

was still comparable between WT and *Fermt3*^{-/-} thymi at P3, the relative numbers of DP T cells decreased and SP CD4 and CD8 T cells increased in P6 thymi of *Fermt3*^{-/-} mice (*Figure 1E,F*). However, despite the shift towards SP T cell populations in P6 *Fermt3*^{-/-} thymi, their absolute numbers were still significantly reduced compared to controls (*Figure 1—figure supplement 1D,E*). The presence of normal relative SP T cell numbers in *Fermt3*^{-/-} thymi until P3 suggests that intrathymic T cell differentiation proceeds independently of kindlin-3. This observation was supported by the normal levels of T cell receptor (TCR), CD3 and costimulatory molecules such as CD5 and CD24 on DP and SP T cells (*Figure 1—figure supplement 1F*).

Thymocyte proliferation depends on kindlin-3 expression

To test whether the number of apoptotic thymocytes is altered within the P3 thymus we immunostained thymic sections for cleaved caspase-3 (*Figure 2A*) and analysed thymocytes by flow cytometry after annexin V and 7-AAD (7-Aminoactinomycin) staining (*Figure 2B*). We found that neither the number (*Figure 2C*) nor the frequency (*Figure 2D*) of apoptotic cells (annexin V$^+$/7-AAD$^-$) was altered in *Fermt3*^{-/-} thymi. Furthermore, the different T cell subsets isolated from WT and *Fermt3*^{-/-} thymi showed a comparable annexin V staining (*Figure 2E*).

Next, we determined thymocyte proliferation by in vivo bromodeoxyuridine (BrdU) labelling, which revealed a significantly reduced number of BrdU positive cells in P3 *Fermt3*^{-/-} thymi both by immunohistochemistry (*Figure 2F,H*) and flow cytometry (*Figure 2G,I*). Notably, reduced proliferation was detected in both the DP and the SP T cell populations (*Figure 2J*). Since thymocyte proliferation relies on proper contact with antigen presenting cells (APC), we tested kindlin-3-deficient T cells for their ability to form immune synapses (IS) with WT DCs. To this end we loaded mature DCs with MOG35-55 peptide and added splenic CD4 T cells from *Fermt3*^{+/fl} and *Fermt3*^{fl/fl} mice, which express a TCR transgene specific for the myelin oligodendrocyte glycoprotein (MOG) 35–55 peptide (*2D2*), a double-fluorescent reporter transgene for measuring Cre activity (mTmG) and the CD4-Cre transgene (*Bettelli et al., 2003*; *Moretti et al., 2013*; *Muzumdar et al., 2007*). After 30 min the T-DC contacts were analysed by immunofluorescence staining. Although *Fermt3*^{-/-} T cells formed fewer contacts with DCs compared to control T cells, recruitment of LFA-1 and actin to the contact area as well as phospho-Tyrosine signals were indistinguishable between them suggesting that *Fermt3*^{-/-} T cells form IS with DCs (*Figure 2—figure supplement 1*). To study APC-induced T cell proliferation in vitro, we co-cultured MOG35-55 peptide-loaded dendritic cells with CSFE-labelled control and kindlin-3-deficient T cells derived from *Fermt3*^{fl/fl}/*CD4-Cre/2D2* mice, and measured CSFE dilution by flow cytometry. In line with the observation that *Fermt3*^{-/-} T cells can form contacts with DCs, a comparable proliferative response was observed when these T cells were stimulated by DCs loaded with high concentration of MOG35-55 peptide or when a strong TCR signal was induced directly with anti-CD3/CD28 antibodies. In contrast, *Fermt3*^{-/-} T cells failed to proliferate when dendritic cells were loaded with lower concentrations of MOG35-55 peptide (*Figure 2K*) indicating that defective integrin-mediated contact between kindlin-3-deficient T cells and APCs causes a reduced proliferative response contributing to thymus atrophy of kindlin-3-deficient mice.

T cell progenitor homing to the postnatal thymus

The reduced CD4 and CD8 DN T cell numbers in *Fermt3*^{-/-} thymi (*Figure 1E,F* and *Figure 1—figure supplement 1D,E*) point to an impaired T cell progenitor homing to the thymus. Upon homing of T cell progenitors to the thymus, they progress through four DN stages before developing into DP cells. To test whether loss of kindlin-3 affects the early and/or late stages of DN development, we separated lineage-positive thymic cells from lineage-negative (Lin^{neg}) DN cells by flow cytometry and gated the latter cell population for high and low CD44 and c-kit expression into DN stage 1 and 2 (DN$_{1-2}$) and DN stage 3 and 4 (DN$_{3-4}$) cells, respectively. In parallel, we gated DN cells for high and low CD44 and CD25 expression to discriminate between the four DN stages. These experiments revealed that the Lin^{neg} DN population was significantly reduced in P3 and P6 thymi and the DN1 and DN2 stage thymocytes were virtually absent from P3 *Fermt3*^{-/-} thymi (*Figure 3A* and *Figure 3—figure supplement 1*). DN1 stage cells are the immediate intrathymic descendants of circulating hematopoietic progenitor cells (Lin^{neg}, c-kit$^+$, Sca-1$^-$ and Sca-1$^+$), which accumulate in the blood circulation of *Fermt3*^{-/-} mice suggesting that extravasation of *Fermt3*^{-/-} T cell progenitors is impaired (*Figure 3B,C*). To test this hypothesis experimentally, we transferred FL cells from E14.5 WT and
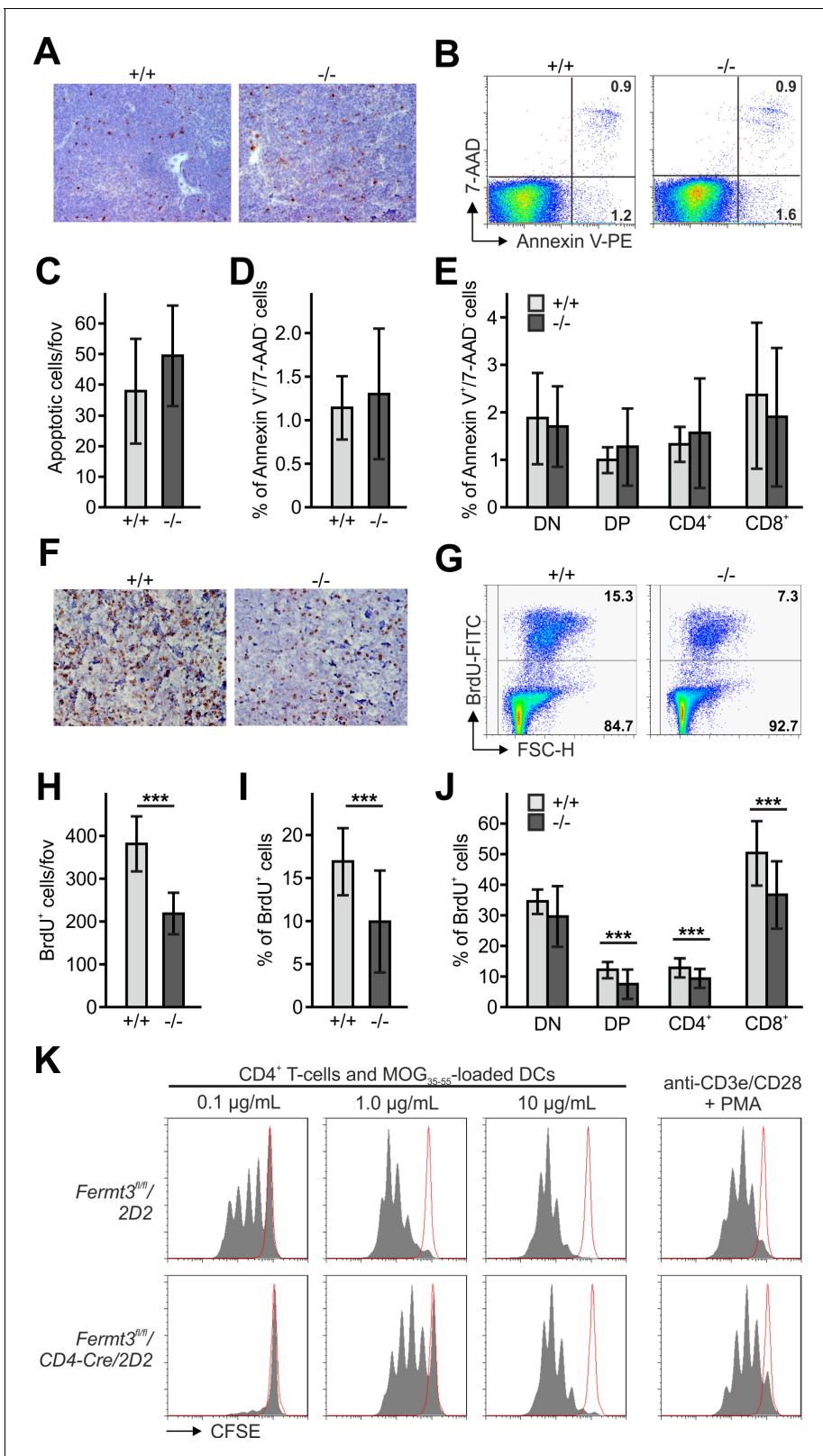
Figure 2. Reduced thymocyte proliferation contributes to thymus atrophy of kindlin-3-deficient mice. (A) Staining for cleaved caspase-3 counterstained with Mayer´s haematoxylin on paraffin sections of *Fermt3*$^{+/+}$ and *Fermt3*$^{-/-}$ P3 thymi. Scale bar 100 μm. (B) Single-cell suspensions of thymocytes from control and *Fermt3*$^{-/-}$ P3 thymi were stained with the apoptotic (Annexin V) and dead cell (7-AAD) markers. Numbers within the FACS blots represent percent of cells within each quadrant. (C) Number of apoptotic cells per field of view (fov) observed in (A). N = 10. Percentage of early apoptotic cells

Figure 2 continued on next page

Fermt3$^{-/-}$ embryos into RAG2-deficient (*Rag2$^{-/-}$*) mice, in which T cell development is blocked at the DN3 stage due to loss of V(D)J rearrangement (*Shinkai et al., 1992*) and analysed size, weight and cellularity of the chimeric thymus and T cell frequency in the peripheral blood 8 to 10 weeks later. The transfer of *Fermt3$^{-/-}$* FL cells failed to reconstitute T cell development in the thymus of *Rag2$^{-/-}$* recipient mice (*Figure 4A–C*), which also contained almost no DN$_{1-2}$ cells (*Figure 4D,E*). Interestingly, a very small number of *Fermt3$^{-/-}$* T cell progenitors entered the *Rag2$^{-/-}$* recipient thymus, differentiated into DN4 cells (*Figure 4D,F*) and produced a small number of circulating CD4 and CD8 T cells, which homed to the spleen of *Rag2$^{-/-}$* mice (*Figure 4G–K*) indicating that kindlin-3 is very important for T cell progenitor homing to the adult thymus, but once in the thymus the progenitor cells differentiate into mature SP T cells that are released into the circulation.

Since kindlin-3-deficient HSCs show an approximately 5-fold reduced homing capacity to the bone marrow, which might eventually impact on T cell progenitor generation (*Ruppert et al., 2015*), we conditionally deleted *Fermt3* by injecting polyIC into *Fermt3$^{fl/fl}$/Mx1-Cre* mice and detected almost no DN (Lin^{neg}) cells in their thymi, whereas control thymi from polyIC-treated *Fermt3$^{fl/fl}$* mice clearly contained a discrete population of DN$_{1-2}$ stage T cells (*Figure 4—figure supplement 1A*). In addition, we generated mixed FL cell chimeras by transferring nine times more *Fermt3$^{-/-}$* FL cells than WT FL cells into lethally irradiated recipient mice and compared their homing capacity to the thymus. To discriminate between both cell populations the WT FL cells were isolated from B6.SJL embryos, which express the CD45.1 allelic variant, while the *Fermt3$^{-/-}$* embryos are from a C57BL/6 background expressing CD45.2. Despite the excess in transferred kindlin-3-deficient FL cells, only around 25% of the DN cells were of CD45.2 origin. As a control, chimeras made from 90% WT CD45.2 cells and 10% WT B6.SJL CD45.1 cells showed the 9:1 ratio in DN and all later T cell stages (*Figure 4—figure supplement 1B*). Moreover, to exclude a defect in a non-hematopoietic cell type as cause for the *Fermt3$^{-/-}$* T cell progenitor homing defect, we analysed thymi from Kindlin-3-EGFP knockin mice, which express kindlin-3 tagged C-terminally with EGFP. Flow cytometry of their thymi revealed that only CD45$^+$ leukocytes were EGFP-positive and that CD31$^+$ endothelial cells and EPCAM$^+$ thymic epithelial cells were EGFP negative (*Figure 4—figure supplement 2*). Altogether, these experiments show that kindlin-3-deficient T cell progenitors have a strong defect in homing to the postnatal and adult thymus and that the homing defect is of hematopoietic origin.

T cell progenitor homing to the thymus primordium

Since thymi of newborn *Fermt3$^{-/-}$* mice lacked DN1 and DN2 cells but contained DN3 and DN4 cells (*Figure 3A*) we surmised that during development significant numbers of T cell progenitors from the FL must be able to colonize the fetal thymus. To test this hypothesis, we determined numbers and locations of CD45$^+$ hematopoietic progenitor cells in sections of the thymus primordium at different time points. In line with previous reports (*Douagi et al., 2000*; *Itoi et al., 2001*), we observed the first wave of WT CD45$^+$ progenitor cells within the perithymic mesenchyme at E11.5, and initial migration into the thymus primordium at E12.0 and scattering throughout the thymus at E12.5 and E13.5 (*Figure 5A–F*). Interestingly, also *Fermt3$^{-/-}$* progenitor cells could be detected in the thymus primordium and the surrounding mesenchyme, however at lower numbers (*Figure 5A–E*). Despite the reduction, CD45$^+$ progenitor cells accumulated at E13.5 in the *Fermt3$^{-/-}$* thymus (*Figure 5D*) and continued
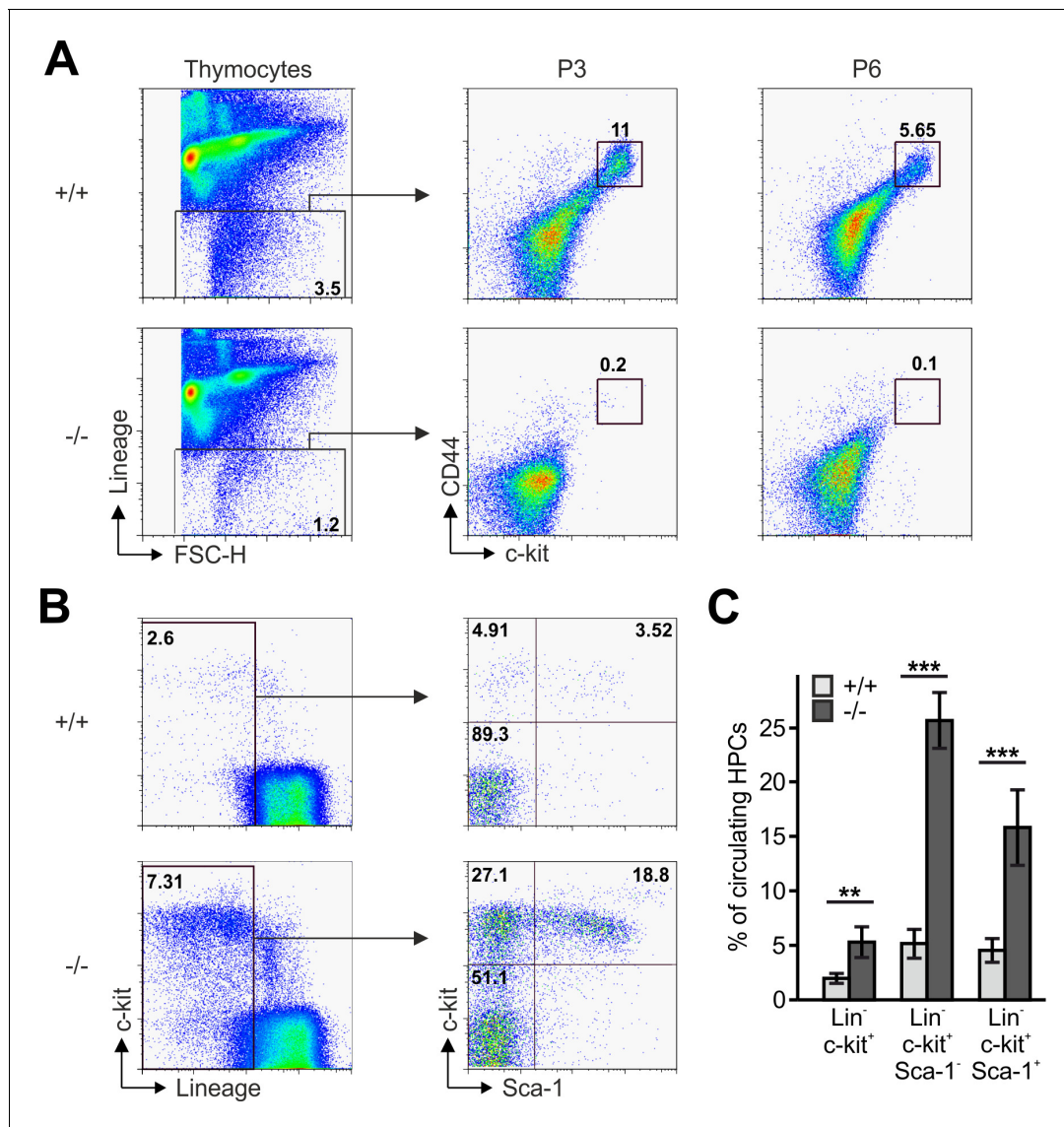
Figure 3. Reduced frequencies of T cell progenitors in *Fermt3*$^{-/-}$ thymi. (**A**) Thymocytes from *Fermt3*$^{+/+}$ and *Fermt3*$^{-/-}$ mice were stained for lineage markers (B220, CD19, TER119, NK1.1, CD11b, Gr-1, CD8α, CD3e, TCRβ, TCRγδ and CD11c), CD44 and c-kit to identify DN$_{1-2}$ (Lin^{neg}, c-kit^{hi}, CD44^{hi}) and the DN$_{3-4}$ (Lin^{neg}, c-kit^{low}, CD44^{low}) populations. (**B and C**) PB from *Fermt3*$^{+/+}$ and *Fermt3*$^{-/-}$ animals (P3) were stained for lineage markers (TER119, B220, CD11b, Gr-1, CD11c, NK1.1, CD4 and CD8α), c-kit and Sca-1 to identify hematopoietic progenitor cells and analysed by flow cytometry. N = 4. Numbers within the representative FACS plots indicate cell percentages. Bars indicate means ± standard errors. **p<0.01; ***p<0.001. See also *Figure 3—figure supplement 1*.

DOI: https://doi.org/10.7554/eLife.35816.006

The following figure supplement is available for figure 3:

Figure supplement 1. Reduced frequencies of T cell prognitors in *Fermt3*$^{-/-}$ thymi.

DOI: https://doi.org/10.7554/eLife.35816.007

developing into DN$_{1-2}$ cells (*Figure 5F*). Strikingly, a dramatic drop in the DN$_{1-2}$ population was observed in *Fermt3*$^{-/-}$ thymi at E15-16 (*Figure 5G,H* and *Figure 5—figure supplement 1A,B*).

Next we tested whether an abnormal *Fermt3*$^{-/-}$ progenitor cell development in the FL or release from the FL into the circulation caused the reduced colonization of the thymus primordium. The flow cytometric analyses revealed that the absolute numbers of Lin^{neg}, c-kit^{hi}, CD45^{+}, PIR^{+} T cell progenitors were comparable between WT and *Fermt3*$^{-/-}$ FLs, while their frequency, due to a decreased cellularity of *Fermt3*$^{-/-}$ FLs, was increased (*Figure 6A–C*). The numbers of circulating WT and *Fermt3*$^{-/-}$ Lin^{neg}, c-kit^{hi}, PIR^{+} T cell progenitors increased between E11.5 to E12. However, while the frequency
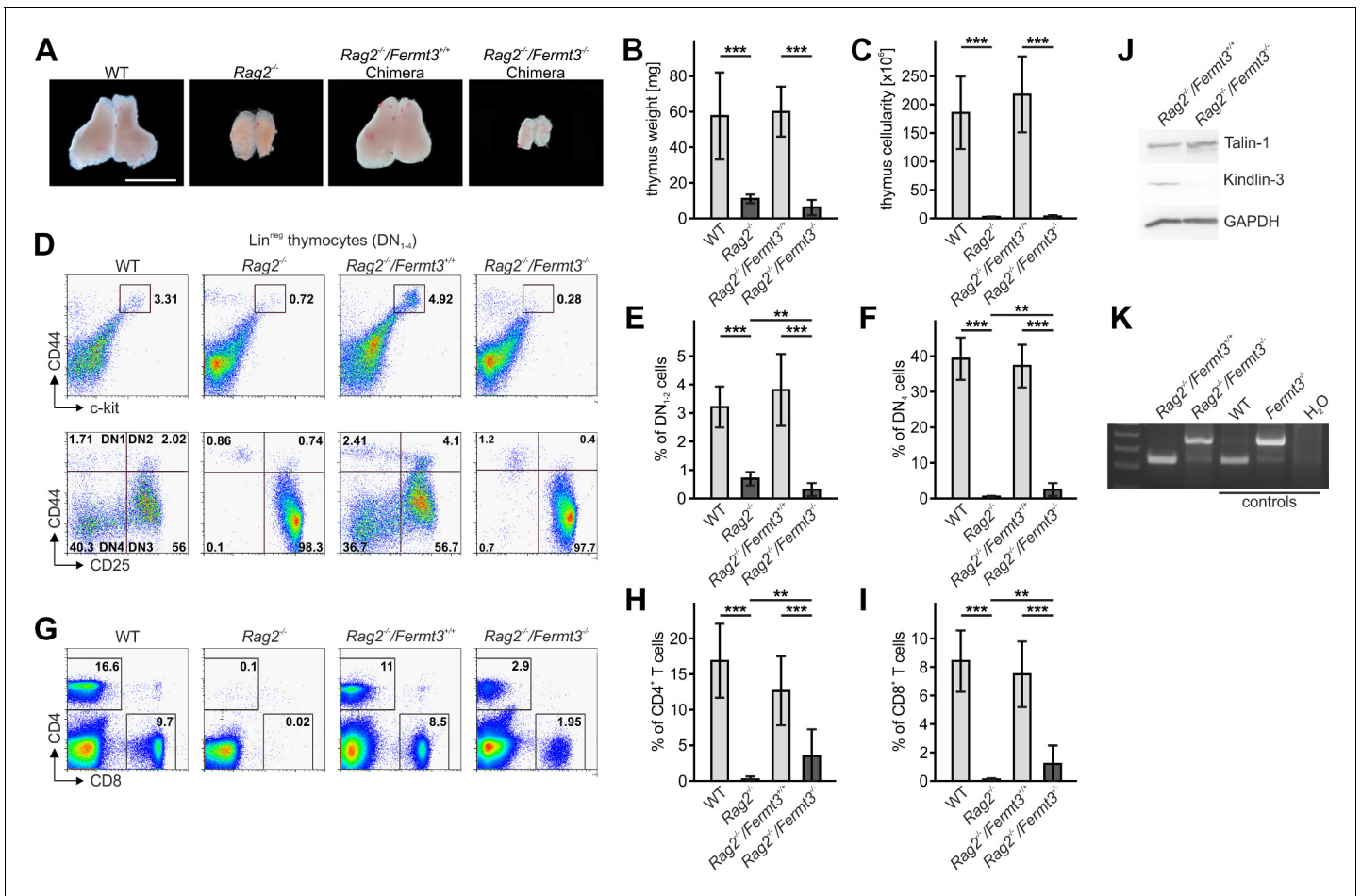
Figure 4. Kindlin-3-deficient T cell progenitors are severely impaired in seeding the adult thymus. (A–C) Images (A), weights (B) and cell numbers (C) of thymi from adult WT and $Rag2^{-/-}$ mice and $Rag2^{-/-}$ mice 10 weeks after reconstitution with $Fermt3^{+/+}$ and $Fermt3^{-/-}$ fetal liver cells. Scale bar 5 mm. N = 10. (D) Single-cell suspensions were stained for lineage markers (B220, CD19, TER119, NK1.1, CD11b, Gr-1, CD11c, CD8α, CD3e, TCRβ, and TCRγδ), c-kit, CD44 and CD25 to identify the DN_{1-2} (Lin^{neg}, c-kit^{hi}, CD44^{hi}) and the DN_{3-4} (Lin^{neg}, c-kit^{low}, CD44^{low}) populations (upper panel), and DN1 (Lin^{neg}, CD44^{hi}, CD25$^-$), DN2 (Lin^{neg}, CD44^{hi}, CD25$^+$), DN3 (Lin^{neg}, CD44^{low}, CD25$^+$) and DN4 (Lin^{neg}, CD44^{low}, CD25$^-$) populations (lower panel) by flow cytometry. Frequencies of DN_{1-2} (E) and DN4 (F) thymocytes. N = 8–10. (G) Analysis of peripheral blood T-lymphocytes. (H and I) Frequencies of circulating CD4$^+$ and CD8$^+$ T cells calculated from flow cytometric analyses shown in (G). N = 10. Numbers within the representative FACS plots indicate cell percentages. (J) Expression of talin-1 and kindlin-3 in CD4$^+$ T cells isolated from the spleen of $Rag2^{-/-}$ mice after reconstitution with $Fermt3^{+/+}$ and $Fermt3^{-/-}$ fetal liver cells. GAPDH serves as loading control. (K) genomic PCR of CD8$^+$ T cells sorted from the spleen of $Rag2^{-/-}/Fermt3^{+/+}$ and $Rag2^{-/-}/Fermt3^{-/-}$ chimeras. Numbers within the representative FACS plots indicate cell percentages. Bars indicate means ± standard errors. **p<0.01; ***p<0.001. See also *Figure 4—figure supplements 1* and *2*.

DOI: https://doi.org/10.7554/eLife.35816.008

The following figure supplements are available for figure 4:

Figure supplement 1. Kindlin-3-deficient T cell progenitors are severely impaired in seeding the adult thymus.
DOI: https://doi.org/10.7554/eLife.35816.009

Figure supplement 2. Kindlin-3-deficient T cell progenitors are severely impaired in seeding the adult thymus.
DOI: https://doi.org/10.7554/eLife.35816.010

of WT T cell progenitors steadily decreased between E12 and E13.5, the T cell progenitors accumulated in the circulation of $Fermt3^{-/-}$ fetuses due to their reduced extravasation from pharyngeal vessels and/or impaired migration towards the thymus primordium (*Figure 6D,E*).

T cell progenitor homing to the thymus is directed by chemokine gradients produced by thymic epithelial cells (*Koch and Radtke, 2011*). Therefore, we decided to test whether $Fermt3^{-/-}$ progenitors are able to sense the chemokine gradient released by thymic lobes in vitro and to invade the thymus. To this end, thymic lobes from WT E15.5 SJL embryos (CD45.1$^+$) were depleted from their
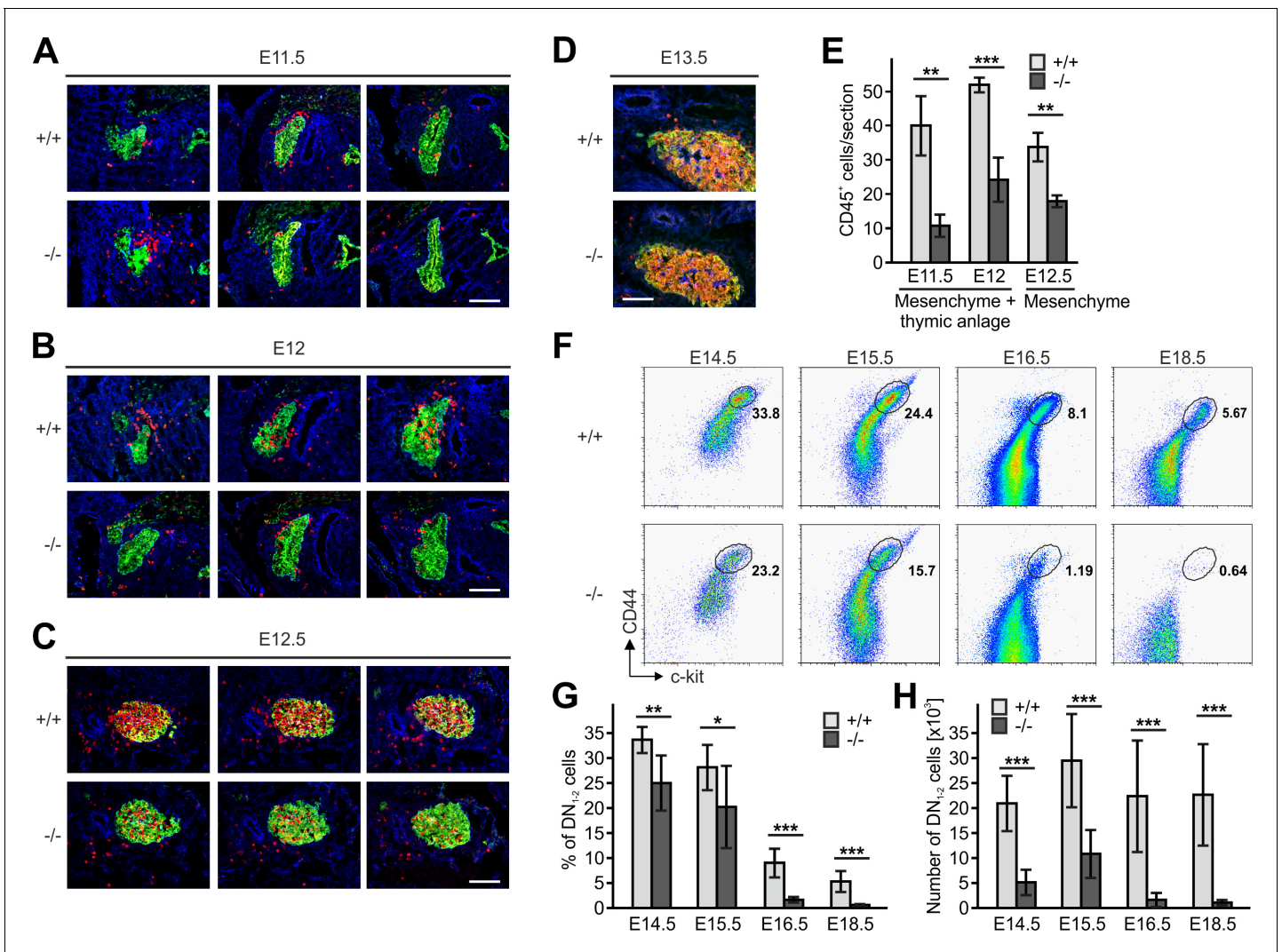
Figure 5. Kindlin-3-independent colonization of the fetal thymus. (A–D) Sagittal sections of whole embryos at gestational ages E11.5 (A), E12 (B), E12.5 (C) and E13.5 (D) were stained for fibronectin (perithymic mesenchyme, blue), cytokeratin (thymic primordium, green) and CD45 (potential T cell progenitor cells, red). Scale bars 100 μm. (E) Numbers of CD45$^+$ cells within the thymic primordium and in the perithymic mesenchyme at the indicated time points. N = 3–4. (F) Representative flow cytometric profiles of fetal thymocytes from control and *Fermt3$^{-/-}$* thymi at the indicated time points stained for lineage markers (B220, CD19, TER119, NK1.1, CD11b, Gr-1, CD11c, CD8α, CD3e, TCRβ, and TCRγδ), c-kit and CD44 to identify the DN$_{1-2}$ (Lin^{neg}, c-kit^{hi}, CD44^{hi}) and the DN$_{3-4}$ (Lin^{neg}, c-kit^{low}, CD44^{low}) populations. Numbers within the representative FACS plots indicate cell percentages. Frequencies (G) and total number (H) of DN$_{1-2}$ cells measured in the flow cytometric analyses shown in (F). N = 7–10 Bars indicate means ± standard errors. *p<0.05; **p<0.01; ***p<0.001. See also *Figure 5—figure supplement 1*.

DOI: https://doi.org/10.7554/eLife.35816.011

The following figure supplement is available for figure 5:

Figure supplement 1. Kindlin-3-independent colonization of the fetal thymus.
DOI: https://doi.org/10.7554/eLife.35816.012

T cells with deoxyguanosine (dGuo) and then positioned in a collagen matrix in close proximity to FL-derived Lin^{neg} cells from WT or *Fermt3$^{-/-}$* E14.5 C57BL/6 (CD45.2$^+$) embryos (*Figure 7A*). Progenitor migration towards the thymic lobes was monitored for 36 to 48 hr by time-lapse video microscopy, which revealed that WT as well as *Fermt3$^{-/-}$* FL cells moved persistently towards the thymic lobes, while migration was not induced when thymic lobes were absent (*Figure 7B*). To further test whether FL-derived T cell progenitor cells had invaded the thymus capsule and developed into mature T cells ex vivo, the lobes were recovered from the collagen matrix and cultured for additional 18 days under conventional fetal thymus organ culture (FTOC) conditions (*Figure 7C*). Consistent
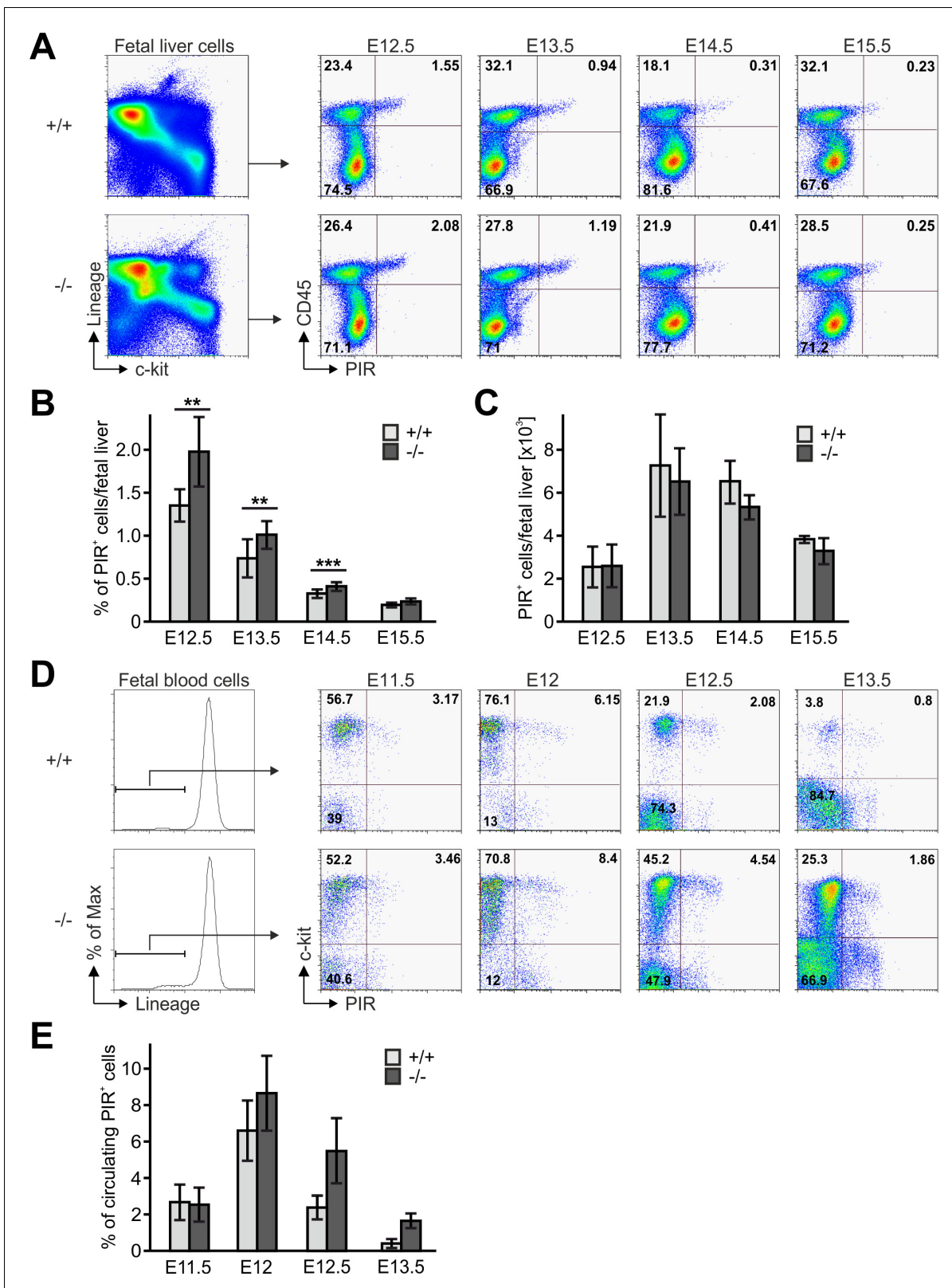
Figure 6. Fetal liver-derived T cell progenitors accumulate in the blood. (**A**) Fetal liver cells from control and *Fermt3$^{-/-}$* embryos from indicated gestational stages were stained for lineage markers (B220, CD19, TER119, NK1.1, Gr-1 and Thy1.2), c-kit, CD45 and PIR and analysed by flow cytometry. Frequencies (**B**) and total numbers (**C**) of PIR$^+$ T cell progenitors per fetal liver. N(E12.5)=7/6; N(E13.5)=8/5; N(E14.5)=10/11; N(E15.5)=4/7. (**D**) FB from *Fermt3$^{+/+}$* and *Fermt3$^{-/-}$* embryos were stained for lineage markers (B220, CD19, TER119, NK1.1, Gr-1 and Thy1.2), c-kit and PIR and analysed by flow
Figure 6 continued on next page

with our in vivo data, CD45.2+ *Fermt3*-/- donor cells normally developed into DP, CD4 and CD8 SP cells (*Figure 7D*).

Altogether these findings indicate that *Fermt3*-/- T cell progenitors normally develop in the FL, are released into the circulation, sense the chemokine gradient, leave the pharyngeal vessel, albeit
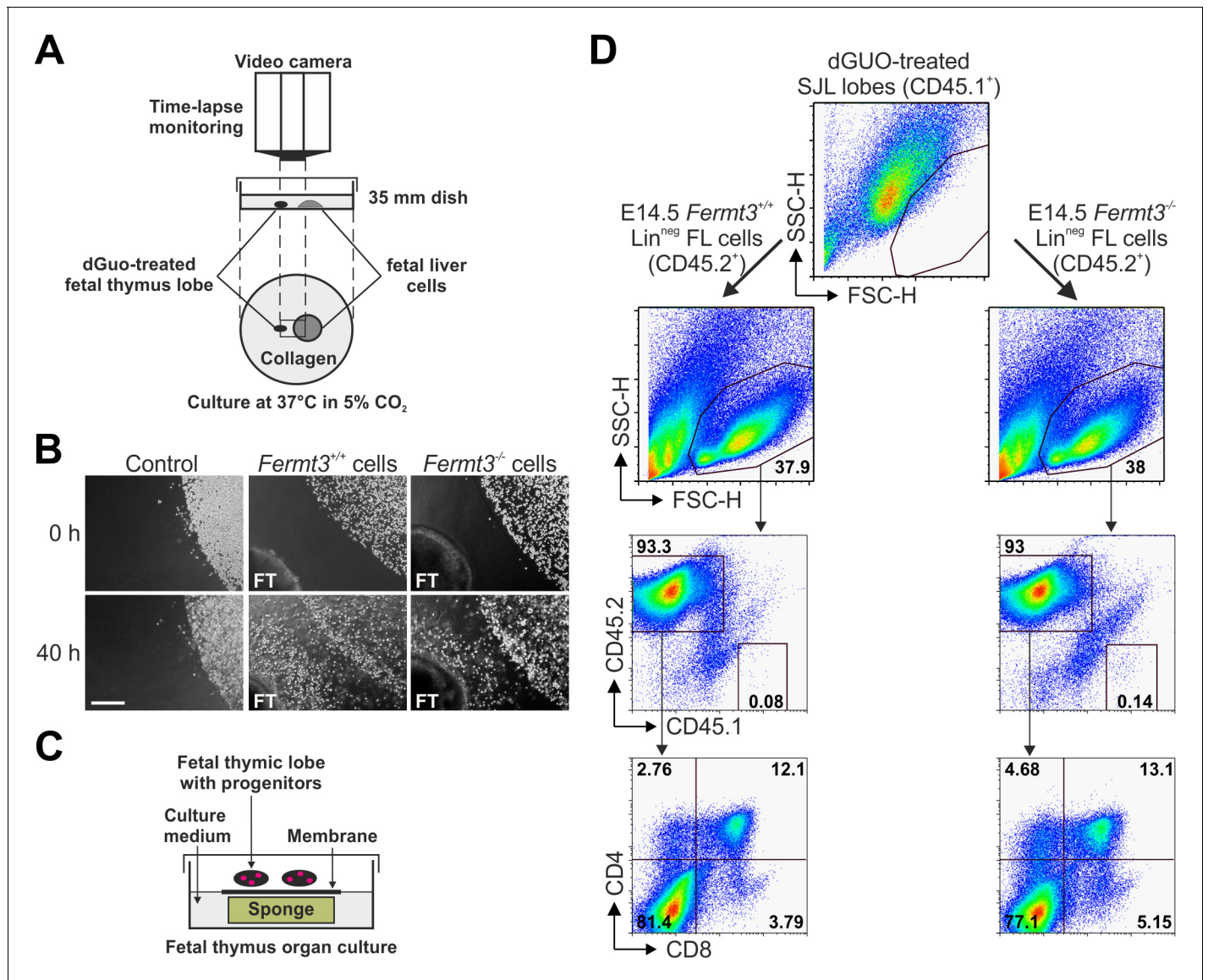
Figure 7. Kindlin-3-deficient T cell progenitors home to the fetal thymus and further develop into SP T cells ex vivo. (A) Schematic description of the thymus attraction experiment. (B) Representative images of the thymus attraction experiment at the beginning and 40 hr after starting the experiment. Lin^neg fetal liver cells from control or *Fermt3*-/- embryos (both CD45.2+) are seen in the upper right corner of the images, a dGuo-treated wild-type fetal thymus lobe (FT, CD45.1+) is located at the lower left corner. Scale bar 250 μm. (C) Schematic description of the fetal thymus organ culture. (D) dGuo-treated fetal thymus lobes seeded with fetal liver cells as performed in (B) were further cultured for 18 days. Cells were stained for CD45.1, CD45.2, CD4, and CD8. Numbers within the representative FACS plots indicate cell percentages.

DOI: https://doi.org/10.7554/eLife.35816.014

less efficiently than WT T cell progenitors, migrate towards the thymus primordium, invade the thymus capsule and differentiate into different T cell subsets.

Blood flow velocity modulates *Fermt3*^{-/-} T cell progenitor adhesion to vascular walls

The differential efficacy of *Fermt3*^{-/-} T cell progenitor homing to the avascular and vascularized thymus was neither due to different kindlin-3 and talin-1 protein levels in lysates from sorted FL-derived T progenitor cells (Lin^{neg}, c-kit^{+}, PIR^{+}) isolated from E13.5 embryos and DN1 cells (Lin^{neg}, CD44^{+}, CD25^{-}) isolated from P6 thymi nor from an upregulation of talin-1 in *Fermt3*^{-/-} PIR^{+} T cell progenitors (*Figure 8A,B*). Flow cytometry also excluded differences in surface expression of α4, αL, β1, β2, β3 and β7 integrins on FL-derived T progenitor cells (Lin[neg], c-kit[+], PIR[+]) (*Figure 8—figure supplement 1*) and BM-derived LSK cells (*Ruppert et al., 2015*). Similarly, the CD31-positive vascular network was indistinguishable in E13.5 and E15.5 thymi from WT and *Fermt3*^{-/-} mice excluding the possibility that a potential kindlin-3 expression in endothelial cells (*Bialkowska et al., 2010*) accounts for the defective homing to the vascularized thymus (data not shown). Since adhesion and extravasation of *Fermt3*^{-/-} T cells can occur on inflamed endothelium expressing high levels of VCAM-1 and ICAM-1 (*Manevich-Mendelson et al., 2009*; *Moretti et al., 2013*), we determined the expression of VCAM-1, ICAM-1 and ICAM-2 by immunostaining and flow cytometry and found them even lower expressed in pharyngeal vessels compared to intrathymic vessels. Thus this also excludes that an elevated adhesion molecule expression on pharyngeal vessels compared to intrathymic vessels accounts for the better adhesion and extravasation (*Figure 8—figure supplement 2A–E*).

Integrin-mediated adhesion of T cells to endothelial adhesion molecules is influenced by the existing vascular shear stress (*Moretti et al., 2013*). We therefore hypothesized that *Fermt3*^{-/-} T cell progenitors show impaired adhesion to the vascular endothelium when blood flow velocity and shear forces increase during intrauterine development. To test this hypothesis, we injected red fluorescent microbeads into the yolk-sac vasculature of E12.5 to E16.5 embryos and measured blood flow velocity by intravital microscopy. We found an increase in blood flow velocity (*Figure 8C*) and shear rates (*Figure 8D*) between E12.5 to 16.5. Accordingly, in vitro flow chamber assays revealed that isolated T cell progenitors (Lin^{neg}, c-kit^{+}, CD45^{+}, Pir^{+}) hardly adhered to P-selectin, CCL21/CCL25 and ICAM-1 (*Figure 8E*), while they readily adhered to P-selectin, CCL21/CCL25 and VCAM-1 in a shear stress-dependent manner. Interestingly, *Fermt3*^{-/-} T cell progenitors adhered to VCAM-1 but displayed a significantly reduced shear force resistance (*Figure 8F*) suggesting that the increase in blood flow velocity and shear forces during fetal development prevents *Fermt3*^{-/-} T cell progenitor adhesion and extravasation at intrathymic vessels. To demonstrate that a strong reduction in kindlin-3 expression only allows adhesion of T cells to the vascular surface at sites with lower shear rates, we adoptively transferred a 1:1 ratio of CSFE and Far Red-labelled CD4 T cells from spleens and LNs of WT and *Fermt3* hypomorphic mice (K3n/-), respectively, into recipient mice and analysed their adhesion to the popliteal LN vasculature by spinning disc confocal microscopy (*Figure 8G,H*). *Fermt3* hypomorphic mice express only 5% kindlin-3 protein and therefore show a strong defect in leukocyte adhesion (*Klapproth et al., 2015*). As expected, we observed a reduced number of adherent *Fermt3* hypomorphic T cells in the LN vasculature compared to WT cells (*Figure 8H,I*). We then injected fluorescent microspheres and measured the blood flow velocities in LN vessel segments and determined shear rates adherent cells were exposed to in those vessels. We found that *Fermt3* hypomorphic cells adhered preferentially in vessel segments where blood flow velocity and shear rates were lower compared to WT T cells. The latter adhered to vessel segments with higher blood flow velocities and shear rates (*Figure 8J,K*). These findings indicate that kindlin-3 is crucial to stabilize integrin-mediated T cell adhesion to vessel walls exposed to high vascular shear forces.

Discussion

In the present study, we used mice lacking the essential integrin regulatory protein kindlin-3 to address the role of integrin-mediated adhesion and signalling during T cell progenitor homing to the thymus and subsequent differentiation within the thymus. We found that in the absence of kindlin-3 a well-organized thymus with normal thymus architecture consisting of the four major compartments (subcapsular zone, cortex, medulla and cortico-medullary junction) is initially formed. The presence and clear separation of DP thymocytes in the cortex from SP CD4 and CD8 T cells in the
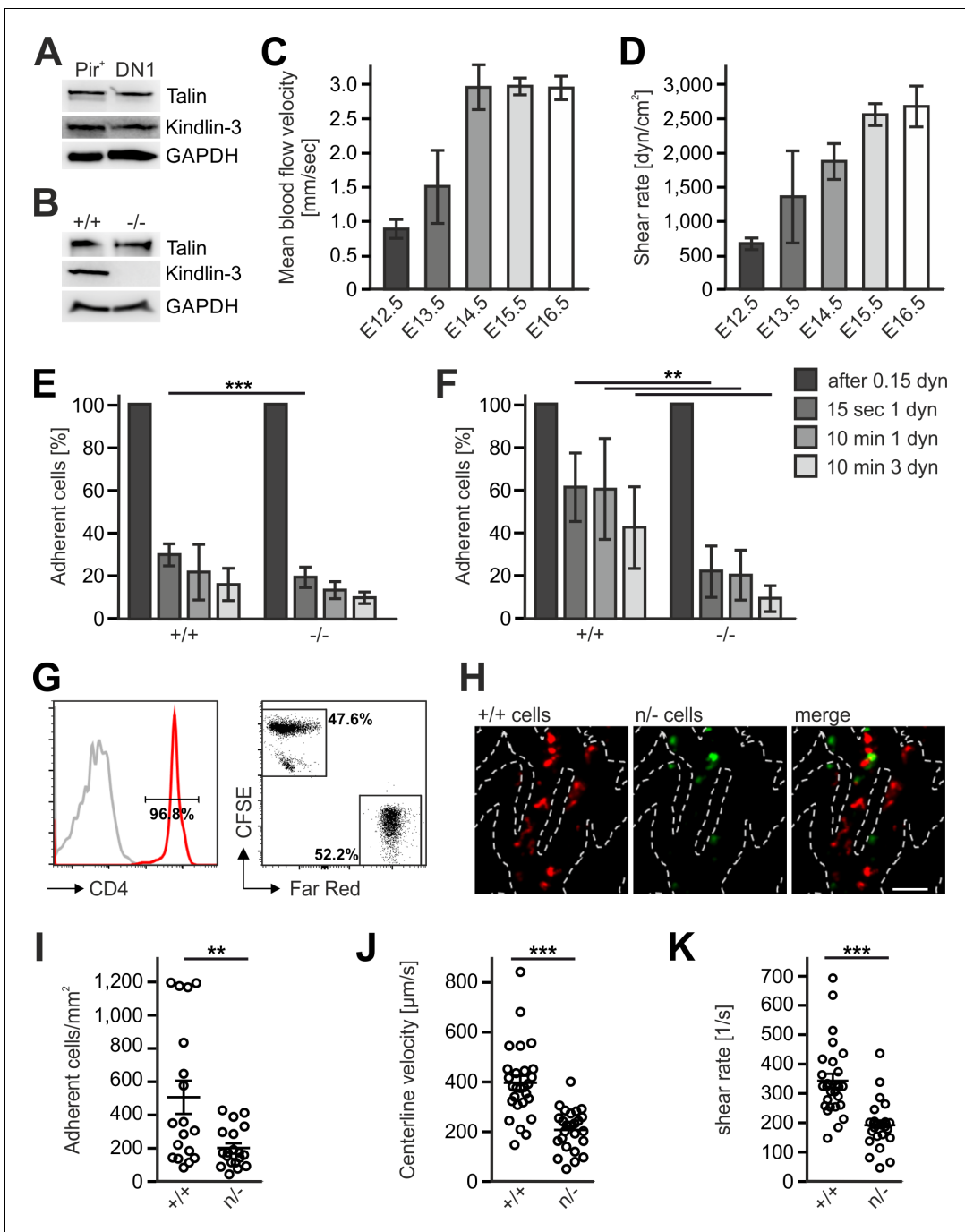
Figure 8. Kindlin-3 is important to stabilize the adhesion of T cell progenitors and mature T cells to vascular integrin ligands when blood flow velocities and shear rate levels increase during development and in vessel segments of higher blood flow within lymph nodes. (A) Talin and kindlin-3 expression in FACS-sorted Pir[+] T cell progenitor cells from WT FL of E13.5 embryos compared to DN1 cells sorted from the thymus of P6 mice. GAPDH served as loading control. (B) Talin and kindlin-3 expression in control and kindlin-3^{-/-} Pir[+] T cell progenitor cells isolated from E13.5 FL. GAPDH served as loading control. Mean blood flow velocities (C) and shear rates (D) within the yolk sac vasculature of E12.5 to E16.5 embryos were determined by intravital microscopy. N = 14/3/8/21/18. (E and F) Relative adhesion of Pir[+] T cell progenitor cells FACS-sorted from the FLs of control and *Fermt3*^{-/-} E13.5 embryos on ICAM-1, P-selectin, CCL21 and CCL25 or on VCAM-1, P-selectin, CCL21 and CCL25 coated ibidi flow chambers with stepwise increasing shear rates. N ≥ 5. Bars indicate means ± standard deviation. (G) Purity of CD4^{+} T cells from WT and *Fermt3* hypomorphic (n/-) mice that have been labelled with CFSE and Far Red and mixed in a 1:1 ratio. Grey line represents isotype control. (H,I) Adhesion of CD4^{+} T cells in vivo. (H) Representative microscopic images of adherent (+/+, red) and (n/-, green) cells in the lymph node vasculature after adoptive transfer. Sum intensity Z projections of confocal stacks are shown. Segmented lines indicate vessel outlines. Scale bar = 50 μm. (I) Quantification of adherent CD4^{+} T cells (N = 18–19 vessels from three mice). (J, K) Microvascular blood flow in the lymph node vasculature. (J) Centerline blood flow velocity and (K) vascular shear rate in LN

Figure 8 continued on next page

Figure 8 continued

microvessel segments (N = 25–27 field of views from three mice). Bars indicate means ± standard deviation. **p<0.01; ***p<0.001. See also *Figure 8—figure supplements 1* and *2*.

The following figure supplements are available for figure 8:

Figure supplement 1. Kindlin-3 is important to stabilize the adhesion of T cell progenitors and mature T cells to vascular integrin ligands when blood flow velocities and shear rate levels increase during development and in vessel segments of higher blood flow within lymph nodes.

Figure supplement 2. Kindlin-3 is important to stabilize the adhesion of T cell progenitors and mature T cells to vascular integrin ligands when blood flow velocities and shear rate levels increase during development and in vessel segments of higher blood flow within lymph nodes.

medulla of postnatal thymi indicate that chemokine-driven migration and positioning of developing T cells to specialized thymic microdomains is not impaired in the absence of kindlin-3 allowing a well-orchestrated developmental maturation from T cell progenitors to mature T cells. Thus, our data indicate that chemokine sensing and leukocyte migration within a 3D environment can occur in the absence of kindlin-3´s role to regulate integrin activity, which is in line with a previous report (*Lämmermann et al., 2008*).

While early thymic development is hardly affected by the lack of kindlin-3, the thymi from kindlin-3 deficient mice began shrinking after birth. We found two main reasons for the thymic atrophy. First, kindlin-3-deficient thymocytes exhibited reduced proliferation rates due to a weakened interaction with thymic APCs. A weakened interaction with APCs was also reported for CD4 T cells isolated from LFA-1 and talin-1 knockout mice to cause reduced T cell proliferation (*Graf et al., 2007*; *Kandula and Abraham, 2004*; *Wernimont et al., 2011*).

Secondly, we observed a severe T cell progenitor homing defect, which becomes apparent at the end of embryogenesis. T cell development in the thymus requires a periodic homing of FL or BM-derived T cell progenitors. The trafficking routes taken by T cell progenitors to the thymus depend on the vascularisation state of the thymus. After vascularization at E15/E16 (*Liu et al., 2006*), FL and later on BM-derived lymphoid progenitors directly enter the thymus at large post-capillary venules at the thymus cortico-medullary junction. This process is critically dependent on kindlin-3. Furthermore, our findings also show that kindlin-3-dependent adhesiveness through multiple integrin classes expressed on T lymphoid progenitors is essential for their homing to the vascularized thymus, while loss of individual integrins either did not or only partially diminish precursor T cell homing (*Scimone et al., 2006*).

Our findings also revealed that kindlin-3-deficient T cell progenitors were able to colonize the non-vascularized thymus primordium and develop into SP CD4 and CD8 T cells that are released into the circulation and found in the spleen. Although early colonization of the thymus anlage was slightly delayed and less efficient, kindlin-3-deficient T cell progenitors were capable to leave the pharyngeal vessels and migrate through the mesenchymal tissue before they reach and enter the thymic anlage. The reduced homing performance of kindlin-3-deficient T cell progenitors was neither due to their reduced production in the FL and/or release into the circulation, nor due to a defect in sensing chemokine cues that direct them towards the thymic primordium. So, we assume that reduced adhesion to the pharyngeal vessel wall accounts for the mild T cell progenitor homing defect of kindlin-3-deficient embryos, an assumption, which is also supported by the accumulation of T cell progenitors in the embryonic circulation.

Why can T cell progenitors extravasate from pharyngeal vessels at early developmental stages but fail to do so from post-capillary venules at the cortico-medullary junction of the vascularized thymus? We cannot fully exclude that differences in the expression of other cell surface receptors, such as CD44 or selectin ligands, may exist between FL and BM-derived T cell progenitors, which allow kindlin-3/integrin independent adhesion and extravasation. However, since impaired adhesion and extravasation becomes evident already before E16, a time point at which BM-derived T cell progenitors have not formed yet, we do not believe that this can explain the homing defect. The fact that FL-derived T cell progenitors are initially capable but later fail to home to the thymus suggests that cell extrinsic rather than cell intrinsic factors are responsible for the impaired colonization. Differences in thymus vascularization might be an obvious possibility, especially since a previous report

suggested kindin-3 expression in endothelial cells (*Bialkowska et al., 2010*). However, we found normal vascularization of the thymus anlage in the absence of kindlin-3 and could show that thymic endothelial cells do not express kindlin-3. Since kindlin-3-deficient thymi exhibited a dramatic drop in the number of DN1 and DN2 cells between E15 to E16, which is the time point when the thymus becomes vascularized (*Liu et al., 2006*), we suggest that differences in the adhesive properties of pharyngeal vs. intrathymic vessels account for this phenomenon. In support of this hypothesis, we reported that kindlin-3-deficient effector T cells can leave the brain vascular system during inflammation when the endothelium expresses ICAM-1 and VCAM-1 at high levels (*Moretti et al., 2013*). Similarly, kindlin-3-deficient effector T cells cannot extravasate from inflamed dermal microvessels but are able to leave postcapillary venules of skin-draining inflamed lymph nodes, probably because the high expression of integrin ligands and P-selectin stabilizes the weak adhesions of kindlin-3-deficient T cells (*Cohen et al., 2013*). However, expression of the integrin ligands ICAM-1/2 and VCAM-1 in pharyngeal vessels is lower than in intrathymic vessels thereby excluding this possibility. Therefore, we reasoned that another mechanism must be responsible for the homing ability of kindlin-3-deficient T cell progenitors to the early thymus.

Beside its role in triggering integrin activation in association with talin-1 (*Ma et al., 2008*; *Montanez et al., 2008*; *Moser et al., 2009a*; *Moser et al., 2009b*; *Moser et al., 2008*), kindlin-3 is important in stabilizing integrin-ligand interactions by promoting integrin clustering (*Feng et al., 2012*; *Ye et al., 2013*). Thus, the gradual T cell progenitor homing defect observed in kindlin-3-deficient mice might be due to instable T cell progenitor/endothelial adhesions, which are unable to withstand increasing shear forces elicited by the maturing blood circulation. Using an intravital microscopy approach we indeed measured an increase in systemic blood flow velocities and shear rates leading to higher hemodynamic forces T-cell progenitors are exposed to during development. In addition, our flow chamber experiments with FL-derived T cell progenitors confirmed this as kindlin-3-deficient cells could adhere to VCAM-1 coated surfaces at low shear stress levels but readily detached at higher shear stress levels when compared to control cells. Moreover, T cells expressing very low kindin-3 levels predominantly adhere to LN vessel segments with lower shear rates than WT T cells. Thus, low shear force conditions may allow adhesion of kindlin-3-deficient T cell progenitors to fetal pharyngeal microvessels, hence enabling their extravasation. However with increasing shear forces at later time points during fetal life, T cell progenitors lacking kindlin-3 and therefore the ability to strengthening integrin-mediated adhesion are not able to efficiently adhere to and migrate out of microvessels into the thymus. The ability to resist low shear forces is also supported by an early report that found high expression of α4β1 on the surface of FL-derived T cell progenitors (*Kawakami et al., 1999*). In addition, we and others have shown that α4β1-mediated adhesiveness to VCAM-1 is less affected by loss of kindlin-3 in contrast to αLβ2 integrin-mediated adhesion to ICAM-1 (*Klapproth et al., 2015*; *Manevich-Mendelson et al., 2009*; *Moretti et al., 2013*). In this respect, it is interesting to note that lack of β1 integrin expression on hematopoietic stem cells (HSC) abolishes their extravasation and homing to the BM (*Potocnik et al., 2000*), whereas kindlin-3-deficient HSCs revealed significantly diminished but not absent homing to the BM (*Ruppert et al., 2015*).

Taken together, our work demonstrates that kindlin-3 is dispensable for integrin-mediated T cell adhesion and signalling at low and indispensable at high vascular shear forces. Furthermore, we also show a general, crucial role of integrins during T cell development and suggest an additional not yet investigated T cell phenotype in LADIII patients.

Materials and methods

Key resources table

Reagent type (species) or resource	Designation	Source or reference	Identifiers	Additional information
Genetic reagent (*M.musculus*)	*Fermt3*^{-/-}	PMID: 18278053	RRID: MGI:2147790	Dr. Reinhard Fässler (Max Planck Institute of Biochemistry)
Genetic reagent (*M.musculus*)	*Fermt3*[flox]	PMID: 24089451	RRID: MGI:5551978	Dr. Reinhard Fässler (Max Planck Institute of Biochemistry)

Continued on next page

Continued

Reagent type (species) or resource	Designation	Source or reference	Identifiers	Additional information
Genetic reagent (*M.musculus*)	*Fermt3*$^{n/-}$	PMID: 26438512	RRID: MGI:3785479	Dr. Reinhard Fässler (Max Planck Institute of Biochemistry)
Genetic reagent (*M.musculus*)	*Rag2*$^{-/-}$	PMID: 1547487	RRID: MGI:1858556	Dr. Frederick W Alt (Howard Hughes Medical Institute)
Genetic reagent (*M.musculus*)	*Mx1-Cre*	PMID: 7660125	RRID: MGI:2176073	Dr. Klaus Rajewsky (Max Delbrück Center for Molecular Medicine)
Genetic reagent (*M.musculus*)	*CD4-Cre*	PMID: 11728338	RRID: MGI: 2386448	Dr. Christopher B. Wilson, (University of Washington)
Genetic reagent (*M.musculus*)	*2D2*	PMID: 12732654	RRID: MGI:3700794	Dr. Vijay K Kuchroo (Center for Neurologic Diseases)
Genetic reagent (*M.musculus*)	*mTmG*	PMID: 17868096	RRID: MGI:3716464	Dr. Liqun Luo (Howard Hughes Medical Institute)
Antibody	anti-B220-biotin	BD Pharmingen	Cat. #: 553085; RRID: AB_394615	FACS (1:200)
Antibody	POD-coupled anti-BrdU	Roche	Cat. #: 11 585 860 001; RRID: AB_514485	IHC (1:30)
Antibody	rabbit anti-mouse cleaved caspase-3	Cell Signalling	Cat. #: 9661; RRID: AB_2341188	IHC (1:100)
Antibody	anti-CD3e	eBioscience	Cat. #: 14-0031-82; RRID: AB_467049	10 µg/ml
Antibody	anti-CD3e-biotin	BD Pharmingen	Cat. #: 553060; RRID: AB_394593	FACS (1:200)
Antibody	anti-CD3-PE	BD Pharmingen	Cat. #: 555275; RRID: AB_395699	FACS (1:200)
Antibody	anti-CD4-biotin	BD Pharmingen	Cat. #: 553649; RRID: AB_394969	FACS (1:200)
Antibody	anti-CD4-FITC	BD Pharmingen	Cat. #: 553651; RRID: AB_394971	FACS (1:200)
Antibody	anti-CD4-PerCP	BD Pharmingen	Cat. #: 550954; RRID: AB_393977	FACS (1:200)
Antibody	anti-CD5-PE	eBioscience	Cat. #: 12-0051-82; RRID: AB_465523	FACS (1:200)
Antibody	anti-CD8α-biotin	BD Pharmingen	Cat. #: 553028; RRID: AB_394566	FACS (1:200)
Antibody	anti-CD8-APC	eBioscience	Cat. #: 17-0081-81; RRID: AB_469334	FACS (1:200)
Antibody	anti-CD8-PE	eBioscience	Cat. #: 12-0081-81; RRID: AB_465529	FACS (1:200)
Antibody	anti-CD11b-biotin	BD Pharmingen	Cat. #: 557395; RRID: AB_2296385	FACS (1:200)
Antibody	anti-CD11c-biotin	BD Pharmingen	Cat. #: 553800; RRID: AB_395059	FACS (1:200)
Antibody	anti-CD16/CD32	BD Pharmingen	Cat. #: 553142; RRID:AB_394657	FACS (1:400)
Antibody	anti-CD19-biotin	eBioscience	Cat. #: 13-0193-82; RRID: AB_657656	FACS (1:200)
Antibody	anti-CD24-PE	BD Pharmingen	Cat. #: 553262; RRID: AB_394741	FACS (1:200)

Continued on next page

Continued

Reagent type (species) or resource	Designation	Source or reference	Identifiers	Additional information
Antibody	anti-CD25-FITC	BD Pharmingen	Cat. #: 553071; RRID: AB_394603	FACS (1:200)
Antibody	anti-CD28	eBioscience	Cat. #: 14-0281-82; RRID: AB_467190	2 µg/ml
Antibody	rat anti-CD31 (PECAM-1)	BD Pharmingen	Cat. #: 557355; RRID: AB_396660	IHC (1:300)
Antibody	anti-CD31-Alexa Fluor 647	Biolegend	Cat. #: 102415; RRID: AB_493411	IHC (1:200)
Antibody	anti-CD31-eFLour450	eBioscience	Cat. #: 48-0311-82; RRID: AB_10598807	FACS (1:200)
Antibody	anti-CD44-PE	BD Pharmingen	Cat. #: 553134; RRID: AB_394649	FACS (1:200)
Antibody	anti-CD45-FITC	eBioscience	Cat. #: 14-0451-82; RRID: AB_467251	IHC (1:100)
Antibody	anti-CD45.2-biotin	BD Pharmingen	Cat. #: 553771; RRID: AB_395040	FACS (1:200)
Antibody	anti-CD45.2-APC	eBioscience	Cat. #: 17-0454-82; RRID: AB_469400	FACS (1:200)
Antibody	hamster anti-CD54 (ICAM)	BD Pharmingen	Cat. #: 553250; RRID: AB_394732	IHC (1:100)
Antibody	goat anti-CD106 (VCAM)	R and D Systems	Cat. #: AF643; RRID: AB_355499	IHC (1:80)
Antibody	anti-c-kit-APC	eBioscience	Cat. #: 17-1171-81; RRID: AB_469429	FACS (1:200)
Antibody	anti-c-kit-PerCP	Biolegend	Cat. #: 105821; RRID: AB_893230	FACS (1:200)
Antibody	mouse anti-pan-cytokeratin	Sigma-Aldrich	Cat. #: C2562; RRID: AB_476839	IHC (1:400)
Antibody	anti-EpCAM-APC-eFlour780	Thermo Fisher Scientific	Cat. #: 47-5791-82; RRID: AB_2573986	FACS (1:200)
Antibody	rat anti-ER-TR4	Eric Vroegindeweij (Princess Maxima center of pediatric oncology)		IHC undiluted
Antibody	rat anti-ER-TR5	Eric Vroegindeweij (Princess Maxima center of pediatric oncology)		IHC undiluted
Antibody	anti-F4/80-biotin	Bio-Rad	Cat. #: MCA497GA; RRID: AB_323806	FACS (1:200)
Antibody	alexa-fluor-488-conjugated anti-Fluorescin IgG	Thermo Fisher Scientific	Cat. #: A-11090; RRID: AB_221562	IHC (1:500)
Antibody	rat anti-ICAM-1 PE	Biolegend	Cat. #:116107; RRID: AB_313698	FACS (1:200)
Antibody	rabbit anti-Fibronectin	Merck Millipore	Cat. #: AB2033; RRID: AB_2105702	IHC (1:300)
Antibody	mouse anti-GAPDH	Merck Millipore	Cat. #: CB1001; RRID: AB_2107426	WB (1:20.000)
Antibody	anti-Gr-1-biotin	BD Pharmingen	Cat. #: 553125; RRID: AB_394641	FACS (1:200)
Antibody	alexa-fluor-546-conjugated anti-goat IgG	Thermo Fisher Scientific	Cat. #: A-11056; RRID: AB_2534103	IHC (1:300)

Continued on next page

Continued

Reagent type (species) or resource	Designation	Source or reference	Identifiers	Additional information
Antibody	alexa-fluor-546-conjugated anti-hamster IgG	Thermo Fisher Scientific	Cat: #: A-21111; RRID: AB_2535760	IHC (1:300)
Antibody	alexa-fluor-546-conjugated anti-mouse IgG	Thermo Fisher Scientific	Cat: #: A-11003; RRID: AB_2534071	IHC (1:300)
Antibody	alexa-fluor-647-conjugated anti-mouse IgG	Thermo Fisher Scientific	Cat: #: A-31571; RRID: AB_162542	IHC (1:300)
Antibody	alexa-fluor-647-conjugated anti-rabbit IgG	Thermo Fisher Scientific	Cat: #: A-21244; RRID: AB_2535812	IHC (1:300)
Antibody	alexa-fluor-488-conjugated anti-rat IgG	Thermo Fisher Scientific	Cat: #: A-11006; RRID: AB_2534074	IHC (1:300)
Antibody	alexa-fluor-647-conjugated anti-rat IgG	Thermo Fisher Scientific	Cat: #: A-21247; RRID: AB_141778	IHC (1:300)
Antibody	anti-Integrin α4-PE	BD Pharmingen	Cat. #: 553157; RRID: AB_394670	FACS (1:200)
Antibody	anti-Integrin αL-PE	BD Pharmingen	Cat. #: 553121; RRID: AB_394637	FACS (1:200)
Antibody	anti-Integrin β1-PE	Biolegend	Cat. #: 102207; RRID: AB_312884	FACS (1:200)
Antibody	anti-Integrin β2-PE	BD Pharmingen	Cat. #: 553293; RRID: AB_394762	FACS (1:200)
Antibody	anti-Integrin β3-PE	eBioscience	Cat. #: 12-0611-81; RRID: AB_465717	FACS (1:200)
Antibody	anti-Integrin β7-PE	BD Pharmingen	Cat. #: 557498; RRID: AB_396735	FACS (1:200)
Antibody	rabbit anti-Kindlin-1	Markus Moser (MPI of Biochemistry)		WB (1:1000)
Antibody	mouse anti-Kindlin-2	Sigma-Aldrich	Cat. # SAB4200525-200UL	WB (1:1000)
Antibody	rabbit anti-Kindlin-3	Markus Moser (MPI of Biochemistry)		WB (1:3000)
Antibody	rabbit anti-pan-laminin	Rupert Timpl		IHC (1:700)
Antibody	anti-LFA-1-PE	BD Pharmingen	Cat. #: 553121; RRID: AB_394637	IF (1:100)
Antibody	anti-NK1.1-biotin	BD Pharmingen	Cat. #: 553163; RRID: AB_394675	FACS (1:200)
Antibody	anti-PIR-APC	eBioscience	Cat. #: 17-3101-82; RRID: AB_1944406	FACS (1:200)
Antibody	anti-PIR-PE	BD Pharmingen	Cat. #: 550349; RRID: AB_393628	FACS (1:200)
Antibody	anti-p-Tyrosine	Santa Cruz Biotechnology	Cat. #: sc-7020; RRID: AB_628123	IF (1:50)
Antibody	anti-Sca-1-PE	eBioscience	Cat. #: 12-5981-82; RRID: AB_466086	FACS (1:200)
Antibody	mouse anti-talin	Sigma-Aldrich	Cat. #: T3287; RRID: AB_477572	WB (1:20.000)
Antibody	anti-TCRβ-PE	eBioscience	Cat. #: 12-5961-82; RRID: AB_466066	FACS (1:200)

Continued on next page

Continued

Reagent type (species) or resource	Designation	Source or reference	Identifiers	Additional information
Antibody	anti-TCRγδ-biotin	BD Pharmingen	Cat. #: 553176; RRID: AB_394687	FACS (1:200)
Antibody	anti-Ter119-biotin	BD Pharmingen	Cat. #: 553672; RRID: AB_394985	FACS (1:200)
Antibody	anti-Thy1.2-biotin	BD Pharmingen	Cat. #: 553001; RRID: AB_394540	FACS (1:200)
Antibody	rat anti-VCAM-1 PE	Biolegend	Cat. #: 105713; RRID: AB_1134166	FACS (1:200)
Peptide, recombinant protein	recombinant mouse CCL21	R and D Systems	Cat. #: 457–6C; Accession #: P84444.1	
Peptide, recombinant protein	recombinant mouse CCL25	R and D Systems	Cat. #: 481-TK; Accession #: O35903.1	
Peptide, recombinant protein	recombinant mouse ICAM-1-FC	R and D Systems	Cat. #: 796-IC; Accession #: Q3U8M7	
Peptide, recombinant protein	MOG35-55	MPI of Biochemistry, Core facility		
Peptide, recombinant protein	recombinant mouse P-Selectin-FC	R and D Systems	Cat. #: 737-PS; Accession #: Q01102	
Peptide, recombinant protein	recombinant mouse VCAM-1-FC	R and D Systems	Cat. #: 643-VM; Accession #: CAA47989	
Commercial assay or kit	PE Annexin V Apoptosis Detection Kit	BD Biosciences	Cat. #: 559763	
Commercial assay or kit	BrdU Flow Kit	BD Pharmingen	Cat. #: 559619; RRID: AB_2617060	
Commercial assay or kit	anti-biotin MicroBeads	Miltenyi	Cat. #: 130-090-485; RRID: AB_244365	
Commercial assay or kit	CD4 T cell isolation kit	Miltenyi	Cat. #: 130-104-454	
Commercial assay or kit	Vectastain Elite ABC HRP Kit, rabbit IgG	VECTOR laboratories	Cat. #: PK-6101; RRID: AB_2336820	
Chemical compound, drug	CellTrace CFSE Cell Proliferation Kit	Thermo Fisher Scientific	Cat. #: C34554	
Chemical compound, drug	Collagenase D	Sigma-Aldrich	Cat. #: C0130	1 mg/ml
Chemical compound, drug	FITC-Dextran	Sigma-Aldrich	Cat. #: FD150S	
Chemical compound, drug	DNaseI	Sigma-Aldrich	Cat. #: D5025	100 U/ml
Chemical compound, drug	dGuo	Sigma-Aldrich	Cat. #: D0901	1.35 mM
Chemical compound, drug	CellTrace Far Red Cell Proliferation Kit	Thermo Fisher Scientific	Cat. #: C34564	1 µM
Chemical compound, drug	FluoSpheres 580/606	Thermo Fisher Scientific	Cat. #: F8821	1 µM
Chemical compound, drug	LPS	Sigma-Aldrich	Cat. #: L2654	1 mg/ml
Chemical compound, drug	poly-L-Lysine	Sigma-Aldrich	Cat. #: P8920	pure

Continued on next page

Continued

Reagent type (species) or resource	Designation	Source or reference	Identifiers	Additional information
Chemical compound, drug	Phalloidin Alexa350	Thermo Fisher Scientific	Cat. #: A22281	IF (1:40)
Chemical compound, drug	PureCol	Advanced BioMatrix	Cat. #: 5005–100 ML	
Chemical compound, drug	Streptavidin Cy3	Jackson Immuno Research	Cat. #: 016-160-084; RRID: AB_2337244	FACS (1:400)
Chemical compound, drug	Streptavidin FITC	Thermo Fisher Scientific	Cat. #: SA10002	FACS (1:200)
Chemical compound, drug	Streptavidin PerCP-Cy5.5	BD Pharmingen	Cat. #: 551419	FACS (1:200)
Software, algorithm	ImageJ	National Institute of Health	RRID:SCR_003070	
Software, algorithm	ImSpector Pro	LaVision BioTec GmbH		
Software, algorithm	Photoshop	Adobe	RRID:SCR_014199	
Software, algorithm	Slidebook 6.0.8 Software	Intelligent Imaging Innovations	RRID:SCR_014300	
Software, algorithm	VirtualDub	GNU General Public License (GPL)		
Other	Glass Bottom Microwell Dishes	MatTek Corporation	Cat. #: P35G-1.5–20 C	
Other	Ibidi flow chambers μ-Slide I 0.8 Luer IbiTreat	Ibidi	Cat. #: 80196	

Mice and chimeras

Fermt3^{-/-} mice have been described previously (**Moser et al., 2008**). All mice were from a mixed 129/SvJ x C57BL/6 background. FL cell chimeras were generated as previously described (**Prümmer and Fliedner, 1986**; **Tulunay et al., 1975**). Briefly, 5–6 × 10^6 cells from the FL of E14.5 embryos were injected into the tail vain of sub-lethally irradiated (1 × 6 Gy) *Rag2*^{-/-} mice (**Shinkai et al., 1992**) and chimeras were analyzed 8 to 10 weeks later. Mixed FL cell chimeras were generated by injection of 5 × 10^6 E14.5 FL cells from WT or *Fermt3*^{-/-} embryos, respectively, which were mixed with E14.5 FL cells from congenic B6.SJL WT embryos in a 9:1 ratio, into lethally irradiated C57BL/6 mice (1 × 7 Gy and 1 × 6 Gy with 4 hr in between). Conditional *Fermt3* deletion was obtained upon two intraperitoneal injections of pI-pC (500 μg/mouse) (GE Healthcare) into *Fermt3*^{fl/fl}/*Mx1-Cre* mice. Pictures of dissected thymi were taken with a ProgRes C14 camera (JenOptic) connected to a Leica MZ FLIII stereomicroscope. All animals were mated and maintained under specific pathogen-free conditions at the animal facility of the Max Planck Institute of Biochemistry. All mouse experiments were performed with the approval of the District Government of Bavaria.

Western blot analysis

Protein lysates were separated on a 10% SDS-PAGE and analyzed by Western blotting using polyclonal rabbit anti-mouse kindlin-1 and kindlin-3 antisera (**Ussar et al., 2008**; **Ussar et al., 2006**), monoclonal mouse anti-kindlin-2 (Sigma), monoclonal mouse anti-talin (Sigma) and mouse anti-GAPDH monoclonal antibody (Calbiochem) with a LAS-4000 imager (Fujifilm).

Multi-color flow cytometry analysis and cell sorting

Multi-color flow-cytometric analysis and cell sorting were performed using FACS-Calibur and FACS-Aria flow cytometers (BD Biosciences), respectively. Data for viable cells, which were determined by forward light scatter and propidium iodide exclusion, were obtained with BD CellQuest Pro software. All antibodies we used were purchased from eBioscience or BD Pharmingen. Lineage negative (Lin[neg]) cell populations were obtained by removal of mature cells using the following cocktails of

biotinylated antibodies: anti-B220, anti-CD19, anti-TER119, anti-NK1.1, anti-CD11b (Mac-1), anti-Gr-1, anti-CD8α, anti-CD3e, anti-TCRβ, anti-TCRγδ and anti-CD11c for fetal and adult thymi; anti-TER119, anti-B220, anti-CD11b, anti-Gr-1, anti-CD11c, anti-NK1.1, anti-CD4 and CD8α for postnatal peripheral blood; anti-B220, anti-CD19, anti-TER119, anti-NK1.1, anti-Gr-1 and anti-Thy1.2 for FL and fetal blood (FB). Cells were then stained either with PerCP-Cy5.5-conjugated or FITC-conjugated Streptavidin and excluded by FL3 or FL1 FACS channels. The resulting Lin^{neg} cell populations were further gated with anti-CD25-FITC, anti-CD44-PE and anti-c-kit-APC for thymocytes; with anti-Sca-1-PE and anti-c-kit-APC for postnatal peripheral blood cells; with anti-CD45-FITC, anti-PIR-PE and anti-c-kit-APC or anti-c-kit-PerCP, anti-PIR-APC and anti-integrin-PE (α4, αL, β1, β2, β3, β7) for FL cells; with anti-PIR-PE and anti-c-kit-APC for FB cells.

Mature T cells were analyzed for surface receptor expression with anti-CD4-FITC, anti CD8-APC, anti-CD3-PE, anti-CD5-PE, anti-CD24-PE and TCRβ-PE.

FL-Lin^{neg} cells used for the time-lapse visualization of thymus attraction (see below) were obtained by negative selection through MACS separation columns with anti-Biotin-coupled magnetic beads according to the manufacturer's instructions (MACS Miltenyi Biotec).

Expression of kindlin-3 in different thymic cell types was analysed by flow cytometry with thymi from Kindlin-3-EGFP knockin mice. A characterization of this mouse strain expressing a kindlin-3-EGFP fusion protein will be described elsewhere. In order to analyse kindlin-3 expression in leukocytes, thymic epithelial cells and endothelial cells, an adult thymus or a pool of 5 E15.5 fetal thymi were squeezed between two glass slides to remove the majority of T cells. The remaining tissue was digested in 1 mg/ml Collagenase D and 100 U/ml DNase I (both from Sigma) in 3% FCS/PBS for 20 to 30 min at 37°C, followed by a Fc-receptor block with anti-CD16/CD32 antibody and incubation with anti-CD31 eFlour450, anti-EpCAM APC eFlour780 (both Invitrogen), anti-CD45.2 APC and anti-CD3 PE antibodies.

Immunofluorescence analysis of embryos and thymi

4% PFA-prefixed, frozen embryos and thymi embedded in Shandon Cryomatrix compound (Thermo Scientific) were first sliced into 8–10 µm thick sections and stained with the following antibodies for the embryos: rabbit anti-fibronectin polyclonal antibody (Chemicon), mouse anti-pan-cytokeratin monoclonal antibody (Sigma), rat anti-CD45-FITC (eBioscience), goat anti-CD106 (VCAM-1, R & D Systems), hamster anti-CD54 (ICAM-1, Pharmingen) and rat anti-CD31 (PECAM-1, Pharmingen) followed by Alexa-Fluor-647-conjugated anti-rabbit IgG, Alexa-Fluor-546-conjugated anti-mouse IgG, Alexa-Fluor-488-conjugated anti-rat IgG, Alexa-Fluor-647-conjugated anti-mouse IgG, Alexa-Fluor-546-conjugated anti-goat IgG, and Fluor-546-conjugated anti-hamster IgG antibodies (Invitrogen); for the thymus: rabbit anti-pan-laminin polyclonal antibody (gift from Rupert Timpl), mouse anti-pan-cytokeratin monoclonal antibody (Sigma), rat anti-CD31 (PECAM-1, Pharmingen), rat anti-CD4-FITC (eBioscience), rat anti-CD8-Biotin (eBioscience), anti-CD106 (VCAM-1, R & D Systems), hamster anti-CD54 (ICAM-1, Pharmingen), rat anti-ER-TR4 and anti-ER-TR5 polyclonal antibodies (kindly provided by Eric Vroegindeweij) followed by Alexa-Fluor-647-conjugated anti-rabbit IgG, Alexa-Fluor-647-conjugated anti-rat IgG, Alexa-Fluor-488-conjugated anti-Fluorescein/Oregon green IgG, Cy3-conjugated Streptavidin (Jackson), Alexa-Fluor-488-conjugated anti-rat IgG, Fluor-546-conjugated anti-goat IgG, and Fluor-546-conjugated anti-hamster IgG antibodies (Invitrogen). Thymic sections were fixed with acetone instead of PFA for anti-ER-TR4 and -TR5 staining.

Relative quantification of ICAM-1 and VCAM-1 expression was performed with directly labelled antibodies: rat anti-ICAM-1-PE, rat anti-VCAM-1-PE and the respective isotypes, rat anti-CD31-Alexa-Fluor 647 (all from Biolegend).

The stained sections were mounted with a fluorescence mounting medium (Elvanol) and images were acquired with a fluorescence microscope (Imager.Z1, Zeiss) and analyzed by the Axio Vision 40 (version 4.8.2.0) software (Zeiss), utilizing 10x, 20x and 40x magnifications.

Immunohistologic analysis of the thymus

4% PFA fixed and paraffin-embedded thymi were sliced into 8 µm tick sections and stained with antibodies. The sections were counterstained with Mayer's haematoxylin (Merck) and mounted in Entellan (Merck). Haematoxylin and Eosin (H/E) staining was performed according to standard protocol.

Images were acquired with the light microscope Axioskop (Zeiss) and analyzed with the Adobe Photoshop software.

Apoptosis assays

Paraffin-embedded thymus sections were stained with rabbit anti-mouse cleaved caspase-3 antibody (Cell Signalling). Apoptotic cells were detected by DAB staining after treatment with the immuno-peroxidase Vectastain ABC system (Vector Laboratories).

Thymocytes from P3 mice were stained with PE-labeled Annexin V and 7-AAD according to the manufacturer's instructions (BD Pharmingen Apoptosis Detection Kit). T cells were additionally stained for anti-CD4-FITC and anti-CD8-APC and analysed by FACS.

Immune synapse analysis

CD4 T cells were purified from spleen by negative selection using biotinylated anti-CD8, anti-B220, anti-Gr-1, anti-F4/80 and anti-Ter119 antibodies and anti-biotin microbeads following the manufacturer's instructions (MACS Miltenyi Biotec). Bone marrow derived, LPS matured dendritic cells were loaded with 1 µg/ml MOG35-55 peptide for 2 hr at a concentration of 10^6 cell/ml. 1×10^5 loaded DCs were mixed with 5×10^5 CD4 T cells in 200 µl R10 medium and seeded on poly-L-Lysine coated glass-bottom dishes (Mattek). Cells were fixed after 30 min by adding 200 µl warm 6% PFA in R10 medium for 20 min at 37°C. After permeabilization with 0.2% Triton X-100 in PBS for 15 min and blocking with 1% BSA for 1 h cells were stained with antibodies against LFA-1 (clone 2D7, BD Biosciences) and p-Tyrosine (PY199, Santa Cruz Biotechnology). Phalloidin Alexa350 was used to visualize actin. Cells were imaged with a Leica TCS SP5 X confocal microscope (Leica Microsystems) equipped with a 63 × NA 1.40 oil objective and Leica Confocal Software (LAS AF). Single channels were imaged sequentially. All pictures were processed with Photoshop (Adobe Systems, San José, California, USA).

Proliferation assays

For in vivo labelling of thymocytes, bromodeoxyuridine (BrdU; 50 µg/gram body weight) was intra-peritoneally injected into P3 mice. One hour after injection, cells were isolated from thymi and stained with FITC-labeled anti-BrdU monoclonal antibody (BD Pharmingen BrdU Flow Kit), anti-CD4-PerCP and anti-CD8-PE antibodies, and analyzed by flow cytometry. Alternatively, paraffin-embedded thymus sections were DAB stained after incubation with a POD-coupled anti-BrdU antibody (Roche).

For the in vitro labeling of control (WT/*2D2*) and kindlin-3-deficient (*Fermt3$^{-/-}$/CD4-Cre/2D2*) CD4$^+$ T cells (*Moretti et al., 2013*), CellTrace CFSE Cell Proliferation Kit (Thermo Fisher) was used to trace dividing cells. Briefly, single cell suspensions from spleens were treated with ammonium-chloridepotassium for RBC lysis and CD4 T cells were sorted using CD4 T cell isolation kit (Milteniy Biotech). T cells were then stained with CFSE according to the manufacturer's instructions and about 5×10^4 T cells per sample were cocultured in triplicate in 96-well round bottom plate with 2×10^4 DCs and increasing concentration of soluble MOG35-55 peptide (0.1, 1 and 10 µg/mL). For T cell stimulation with anti-CD3e and anti-CD28 Abs, 2×10^5 CFSE-labelled cells per sample were cultured in wells pre-coated for 1 hr at 37°C with anti-CD3e (10 µg/ml, eBioscience), with soluble anti-CD28 (2 µg/ml, eBioscience) and PMA (20 ng/ml). Proliferation was analysed by FACS after 3 days of incubation in R10 (RPMI-1640, 10% FCS, 1x Penicillin-Streptomycin) at 37°C.

Time-lapse visualization of thymus attraction

Time-lapse imaging of horizontal cell migration to fetal thymus lobes was recorded as previously described (*Liu et al., 2005*; *Ueno et al., 2005*). Briefly, 10 µL of freshly neutralized collagen solution (1.72 mg/mL PureCol, Advanced BioMatrix, in RPMI 1640-based culture medium) containing 1–2 × 10^5 FL-Lin^{neg} cells from either *Fermt3$^{+/+}$* or *Fermt3$^{-/-}$* C57BL/6 (CD45.2$^+$) animals was placed in a 35 mm plastic dish and solidified at 37°C for 10 min. An E15.5 fetal thymus lobe from wild-type SJL (CD45.1$^+$) mouse, pre-treated for 6 days with 1.35 mM 2-deoxyguanosine (dGuo; Sigma) was positioned approximately 0.5 mm away from the cell spot. The culture was submerged in 1.72 mg/mL collagen medium and solidified at 37°C for 30 min. The dish was placed in 5% CO_2 under an Axio-vert 40 CFL microscope (Zeiss) equipped with a digital CCD camera. The culture was time-lapse

monitored for 36 to 48 hr. After colonization, fetal thymus lobes were removed from the collagen gel, rinsed, and further cultured for 18 days under conventional organ culture conditions (see below). Thymi were than pooled, squeezed through a cell strainer and the resulting single cell suspensions were stained with anti-CD45.2 to identify FL cell-derived thymocytes and further gated for anti-CD4-FITC and anti-CD8-APC.

Fetal Thymus Organ Culture
Seeded thymus lobes were cultured on 0.8 µm isopore membrane filters (Millipore) supported by a Gelfoam sponge (Pfizer) at an interface between 5% CO_2-humidified air and RPMI 1640-based culture medium containing 10% FCS, 100 U/ml penicillin and 100 µg/ml streptomycin (PAA), 2 mM L-glutamine (PAA), 1X non-essential amino acids (Gibco), 1 mM sodium pyruvate (Gibco), 10 mM HEPES, 50 µM 2-mercaptoethanol (Sigma). Details have been described (*Ueno et al., 2005*).

Blood flow velocity measurement
Blood flow velocity measurements were performed in the fetal yolk-sac vasculature of E12.5 to E16.5 fetuses as described (*Margraf et al., 2017*). Briefly, pregnant WT mice were anesthetised and fetuses surrounded by the yolk sac and still connected to the placenta were surgically exteriorized and placed on a modified intravital microscopy stage. Manually prepared glass microcapillaries (Clark Capillaries GCI150TF-10, Clark Electromedical Instruments, Pangbourne Reading) were used to inject 4 µl of a 5% FITC dextrane solution (FD150S, Sigma-Aldrich, Taufkirchen, Germany) with 1 µl of red fluorescent microspheres (FluoSpheres polystyrene microspheres 1,0 µm red fluorescent 580/605; Invitrogen) into the fetal vasculature. Imaging was performed using an in vivo microscope setup (Olympus BX1, Olympus, Hamburg, Germany) equipped with appropriate filter sets and a double-flash device (Rapp Optoelectronics, Hamburg, Germany). Images were recorded using a 60x objective (Olympus LUM Plan FI/IR 60x/0.90W) with setup specific CCD-cameras (Kappa CF5 HS; Kappa Optronics GmbH, Gleichen, Germany, and LaVision Imager ProX pco.1600L, LaVision GmbH, Goettingen, Germany) and recorded utilizing VirtualDub (www.virtualdub.org) and Imspector Pro Software (Lavision BioTec GmbH, Bielefeld, Germany). Analysis was performed using ImageJ (National Institute of Health). Vessel diameters were chosen between 20 and 50 µm.

Flow chamber assays
Flow chamber assays were performed with the ibidi pump system (Martinsried, Germany). Ibidi flow chambers (µ-Slide I 0.8 Luer ibiTreat) were coated with 10 µg/ml recombinant mouse (rm) ICAM-1-Fc or rmVCAM-1-Fc, 10 µg/ml rmP-selectin-Fc, 5 µg/ml rmCCL21 and 5 µg/ml rmCCL25 (all from R & D systems) over night at 4°C. After blocking for 1 hr with 1% casein (Thermo Fisher Scientific) at room temperature, the channels were filled with control or *Fermt3*$^{-/-}$ Pir$^+$ T cell progenitors sorted from E13.5 fetal livers. After 3 min incubation without flow, slow flow of approximately 0.15 dyn/cm^2 was applied for 3 min followed by increasing flow of 1 and 3 dyn/cm^2 for 10 min each. Pictures were taken every 5 s for a total of 25 min at an Axiovert 40 CFL microscope (Zeiss) equipped with a digital CCD camera and a 10 x objective. The number of cells that were adherent immediately before the start of the fast flow was set to 100%. Cells that did not change position within 10 s were considered to be firmly adherent.

Live cell imaging of T cell adhesion within the lymph node vasculature and flow in vivo
CD4 T cells were isolated from spleen by negative selection as described above. Anaesthetized mice were injected intravenously with a 1:1 mixture of CFSE and Far Red labelled WT and *Fermt3* hypomorphic CD4 T cells. The hair of the hind legs was removed and mice were placed into an imaging chamber with integrated heating plate. In a dorsal approach the skin of the hind legs was cut and the popliteal lymph nodes were exposed. To reveal the superficial vessels of the lymph nodes, they were fixed to the biceps femoris muscle using Histoacryl tissue adhesive (B. Braun). PBS-soaked batting was placed around the legs to keep the tissue moist. The lymph nodes were covered with a cover glass, which was topped with PBS to facilitate imaging. Time-lapse video microscopy was performed using an upright spinning disk confocal microscope (Examiner, Zeiss, Germany) equipped with a confocal scanner unit CSU-X1 (Yokogawa Electric Corporation, Japan), an EMCCD camera

(Evolve, Photometrics, USA) and a 20x/1.0NA water immersion objective (Zeiss, Germany). 4D images (30 z-stacks with a step size of 4 μm and an average time lapse interval of 42 s) were acquired by using two lasers with an excitation wavelength of 488 nm and 640 nm. Adhesion was analyzed by generating sum projections of z-stacks over time using Slidebook 6.0.8 Software (3i, USA). The number of adherent leukocytes was determined as cells attached to the same position for more than 1 min using Fiji/ImageJ software (NIH, USA). Centerline blood flow velocities in the same vessels were obtained upon subsequent intravenous injection of 10^7 fluorescent microspheres (1 μm in diameter; FluoSpheres 580/605, Invitrogen) by measuring frame-to-frame displacement of single beads in LN microvessel segments. Images of one plane with an average time lapse interval of 66.5 ms were acquired for one minute using one laser with an excitation wavelength of 561 nm. Wall shear rates were calculated as previously described (*Sperandio et al., 2006*).

Statistic analysis

Means, standard deviations and statistical comparisons with Student's t-test (*$p < 0.05$, **$p < 0.01$, ***$p < 0.001$) were made using Microsoft Excel software.

Ackowledgments

Additional information

Competing interests

Reinhard Fässler: Reviewing editor, *eLife*. The other authors declare that no competing interests exist.

Funding

Author contributions

Federico Andrea Moretti, Investigation, Writing—original draft, Carried out most experiments and data analyses, Evaluated and interpreted the data; Sarah Klapproth, Investigation, Carried out most experiments and data analyses, Evaluated and interpreted the data; Raphael Ruppert, Investigation, Generated and analysed chimeric mice; Andreas Margraf, Investigation, Measured blood flow velocities and shear rates in the yolk sac vasculature; Jasmin Weber, Robert Pick, Investigation, Performed and analysed the lymph node homing experiments; Christoph Scheiermann, Supervision, Investigation, Supervised the lymph node homing experiments and measured integrin ligand expression in

the vasculature; Markus Sperandio, Supervision, Supervised the blood flow and shear rate measurements in the yolk sac vasculature; Reinhard Fässler, Supervision, Funding acquisition, Writing—review and editing; Markus Moser, Supervision, Funding acquisition, Investigation, Writing—original draft, Writing—review and editing

Author ORCIDs
Federico Andrea Moretti https://orcid.org/0000-0003-3187-3683
Markus Sperandio https://orcid.org/0000-0002-7689-3613
Markus Moser https://orcid.org/0000-0001-8825-5566

Decision letter and Author response
Decision letter https://doi.org/10.7554/eLife.35816.021
Author response https://doi.org/10.7554/eLife.35816.022

Additional files

Supplementary files
• Transparent reporting form
DOI: https://doi.org/10.7554/eLife.35816.018

Data availability
All data generated or analysed during this study are included in the manuscript and supporting files.

References

Arroyo AG, Yang JT, Rayburn H, Hynes RO. 1996. Differential requirements for alpha4 integrins during fetal and adult hematopoiesis. *Cell* **85**:997–1008. DOI: https://doi.org/10.1016/S0092-8674(00)81301-X, PMID: 8674127

Bettelli E, Pagany M, Weiner HL, Linington C, Sobel RA, Kuchroo VK. 2003. Myelin oligodendrocyte glycoprotein-specific T cell receptor transgenic mice develop spontaneous autoimmune optic neuritis. *The Journal of Experimental Medicine* **197**:1073–1081. DOI: https://doi.org/10.1084/jem.20021603, PMID: 12732654

Bialkowska K, Ma YQ, Bledzka K, Sossey-Alaoui K, Izem L, Zhang X, Malinin N, Qin J, Byzova T, Plow EF. 2010. The integrin co-activator Kindlin-3 is expressed and functional in a non-hematopoietic cell, the endothelial cell. *Journal of Biological Chemistry* **285**:18640–18649. DOI: https://doi.org/10.1074/jbc.M109.085746, PMID: 20378539

Boehm T, Bleul CC. 2006. Thymus-homing precursors and the thymic microenvironment. *Trends in Immunology* **27**:477–484. DOI: https://doi.org/10.1016/j.it.2006.08.004, PMID: 16920024

Bungartz G, Stiller S, Bauer M, Müller W, Schippers A, Wagner N, Fässler R, Brakebusch C. 2006. Adult murine hematopoiesis can proceed without beta1 and beta7 integrins. *Blood* **108**:1857–1864. DOI: https://doi.org/10.1182/blood-2005-10-007658, PMID: 16735603

Cai AQ, Landman KA, Hughes BD, Witt CM. 2007. T cell development in the thymus: from periodic seeding to constant output. *Journal of Theoretical Biology* **249**:384–394. DOI: https://doi.org/10.1016/j.jtbi.2007.07.028, PMID: 17869276

Cohen SJ, Gurevich I, Feigelson SW, Petrovich E, Moser M, Shakhar G, Fassler R, Alon R. 2013. The integrin coactivator Kindlin-3 is not required for lymphocyte diapedesis. *Blood* **122**:2609–2617. DOI: https://doi.org/10.1182/blood-2013-04-495036, PMID: 23980064

Douagi I, André I, Ferraz JC, Cumano A. 2000. Characterization of T cell precursor activity in the murine fetal thymus: evidence for an input of T cell precursors between days 12 and 14 of gestation. *European Journal of Immunology* **30**:2201–2210. DOI: https://doi.org/10.1002/1521-4141(2000)30:18<2201::AID-IMMU2201>3.0.CO;2-J, PMID: 10940911

Feng C, Li YF, Yau YH, Lee HS, Tang XY, Xue ZH, Zhou YC, Lim WM, Cornvik TC, Ruedl C, Shochat SG, Tan SM. 2012. Kindlin-3 mediates integrin αLβ2 outside-in signaling, and it interacts with scaffold protein receptor for activated-C kinase 1 (RACK1). *Journal of Biological Chemistry* **287**:10714–10726. DOI: https://doi.org/10.1074/jbc.M111.299594, PMID: 22334666

Foss DL, Donskoy E, Goldschneider I. 2001. The importation of hematogenous precursors by the thymus is a gated phenomenon in normal adult mice. *The Journal of Experimental Medicine* **193**:365–374. DOI: https://doi.org/10.1084/jem.193.3.365, PMID: 11157056

Georges-Labouesse E, Messaddeq N, Yehia G, Cadalbert L, Dierich A, Le Meur M. 1996. Absence of integrin alpha 6 leads to epidermolysis bullosa and neonatal death in mice. *Nature Genetics* **13**:370–373. DOI: https://doi.org/10.1038/ng0796-370, PMID: 8673141

Graf B, Bushnell T, Miller J. 2007. LFA-1-mediated T cell costimulation through increased localization of TCR/class II complexes to the central supramolecular activation cluster and exclusion of CD45 from the immunological synapse. *The Journal of Immunology* **179**:1616–1624. DOI: https://doi.org/10.4049/jimmunol.179.3.1616, PMID: 17641028

Itoi M, Kawamoto H, Katsura Y, Amagai T. 2001. Two distinct steps of immigration of hematopoietic progenitors into the early thymus anlage. *International Immunology* **13**:1203–1211. DOI: https://doi.org/10.1093/intimm/13.9.1203, PMID: 11526101

Jotereau F, Heuze F, Salomon-Vie V, Gascan H. 1987. Cell kinetics in the fetal mouse thymus: precursor cell input, proliferation, and emigration. *Journal of Immunology* **138**:1026–1030. PMID: 2879866

Kandula S, Abraham C. 2004. LFA-1 on CD4+ T cells is required for optimal antigen-dependent activation in vivo. *The Journal of Immunology* **173**:4443–4451. DOI: https://doi.org/10.4049/jimmunol.173.7.4443, PMID: 15383575

Kawakami N, Nishizawa F, Sakane N, Iwao M, Tsujikawa K, Ikawa M, Okabe M, Yamamoto H. 1999. Roles of integrins and CD44 on the adhesion and migration of fetal liver cells to the fetal Thymus. *Journal of Immunology* **163**:3211–3216.

Klapproth S, Moretti FA, Zeiler M, Ruppert R, Breithaupt U, Mueller S, Haas R, Mann M, Sperandio M, Fässler R, Moser M. 2015. Minimal amounts of kindlin-3 suffice for basal platelet and leukocyte functions in mice. *Blood* **126**:2592–2600. DOI: https://doi.org/10.1182/blood-2015-04-639310, PMID: 26438512

Koch U, Radtke F. 2011. Mechanisms of T cell development and transformation. *Annual Review of Cell and Developmental Biology* **27**:539–562. DOI: https://doi.org/10.1146/annurev-cellbio-092910-154008, PMID: 21740230

Koni PA, Joshi SK, Temann UA, Olson D, Burkly L, Flavell RA. 2001. Conditional vascular cell adhesion molecule 1 deletion in mice: impaired lymphocyte migration to bone marrow. *The Journal of experimental medicine* **193**:741–754. PMID: 11257140

Krüger M, Moser M, Ussar S, Thievessen I, Luber CA, Forner F, Schmidt S, Zanivan S, Fässler R, Mann M. 2008. SILAC mouse for quantitative proteomics uncovers kindlin-3 as an essential factor for red blood cell function. *Cell* **134**:353–364. DOI: https://doi.org/10.1016/j.cell.2008.05.033, PMID: 18662549

Kuijpers TW, van de Vijver E, Weterman MA, de Boer M, Tool AT, van den Berg TK, Moser M, Jakobs ME, Seeger K, Sanal O, Unal S, Cetin M, Roos D, Verhoeven AJ, Baas F. 2009. LAD-1/variant syndrome is caused by mutations in FERMT3. *Blood* **113**:4740–4746. DOI: https://doi.org/10.1182/blood-2008-10-182154, PMID: 19064721

Lämmermann T, Bader BL, Monkley SJ, Worbs T, Wedlich-Söldner R, Hirsch K, Keller M, Förster R, Critchley DR, Fässler R, Sixt M. 2008. Rapid leukocyte migration by integrin-independent flowing and squeezing. *Nature* **453**:51–55. DOI: https://doi.org/10.1038/nature06887, PMID: 18451854

Ley K, Laudanna C, Cybulsky MI, Nourshargh S. 2007. Getting to the site of inflammation: the leukocyte adhesion cascade updated. *Nature Reviews Immunology* **7**:678–689. DOI: https://doi.org/10.1038/nri2156, PMID: 17717539

Liu C, Ueno T, Kuse S, Saito F, Nitta T, Piali L, Nakano H, Kakiuchi T, Lipp M, Hollander GA, Takahama Y. 2005. The role of CCL21 in recruitment of T-precursor cells to fetal thymi. *Blood* **105**:31–39. DOI: https://doi.org/10.1182/blood-2004-04-1369, PMID: 15358618

Liu C, Saito F, Liu Z, Lei Y, Uehara S, Love P, Lipp M, Kondo S, Manley N, Takahama Y. 2006. Coordination between CCR7- and CCR9-mediated chemokine signals in prevascular fetal thymus colonization. *Blood* **108**:2531–2539. DOI: https://doi.org/10.1182/blood-2006-05-024190, PMID: 16809609

Ma YQ, Qin J, Wu C, Plow EF. 2008. Kindlin-2 (Mig-2): a co-activator of beta3 integrins. *The Journal of Cell Biology* **181**:439–446. DOI: https://doi.org/10.1083/jcb.200710196, PMID: 18458155

Malinin NL, Zhang L, Choi J, Ciocea A, Razorenova O, Ma YQ, Podrez EA, Tosi M, Lennon DP, Caplan AI, Shurin SB, Plow EF, Byzova TV. 2009. A point mutation in KINDLIN3 ablates activation of three integrin subfamilies in humans. *Nature Medicine* **15**:313–318. DOI: https://doi.org/10.1038/nm.1917, PMID: 19234460

Manevich-Mendelson E, Feigelson SW, Pasvolsky R, Aker M, Grabovsky V, Shulman Z, Kilic SS, Rosenthal-Allieri MA, Ben-Dor S, Mory A, Bernard A, Moser M, Etzioni A, Alon R. 2009. Loss of Kindlin-3 in LAD-III eliminates LFA-1 but not VLA-4 adhesiveness developed under shear flow conditions. *Blood* **114**:2344–2353. DOI: https://doi.org/10.1182/blood-2009-04-218636, PMID: 19617577

Margraf A, Nussbaum C, Rohwedder I, Klapproth S, Kurz ARM, Florian A, Wiebking V, Pircher J, Pruenster M, Immler R, Dietzel S, Kremer L, Kiefer F, Flemmer AW, Quackenbush E, von Andrian UH, Sperandio M. 2017. Maturation of platelet function during murine fetal development in vivo. *Arteriosclerosis, Thrombosis, and Vascular Biology* **37**:1076–1086. DOI: https://doi.org/10.1161/ATVBAHA.116.308464, PMID: 28428216

Montanez E, Ussar S, Schifferer M, Bösl M, Zent R, Moser M, Fässler R. 2008. Kindlin-2 controls bidirectional signaling of integrins. *Genes & Development* **22**:1325–1330. DOI: https://doi.org/10.1101/gad.469408, PMID: 18483218

Moretti FA, Moser M, Lyck R, Abadier M, Ruppert R, Engelhardt B, Fässler R. 2013. Kindlin-3 regulates integrin activation and adhesion reinforcement of effector T cells. *PNAS* **110**:17005–17010. DOI: https://doi.org/10.1073/pnas.1316032110, PMID: 24089451

Mory A, Feigelson SW, Yarali N, Kilic SS, Bayhan GI, Gershoni-Baruch R, Etzioni A, Alon R. 2008. Kindlin-3: a new gene involved in the pathogenesis of LAD-III. *Blood* **112**:2591. DOI: https://doi.org/10.1182/blood-2008-06-163162, PMID: 18779414

Moser M, Nieswandt B, Ussar S, Pozgajova M, Fässler R. 2008. Kindlin-3 is essential for integrin activation and platelet aggregation. *Nature Medicine* **14**:325–330. DOI: https://doi.org/10.1038/nm1722, PMID: 18278053

Moser M, Bauer M, Schmid S, Ruppert R, Schmidt S, Sixt M, Wang HV, Sperandio M, Fässler R. 2009a. Kindlin-3 is required for beta2 integrin-mediated leukocyte adhesion to endothelial cells. *Nature Medicine* **15**:300–305. DOI: https://doi.org/10.1038/nm.1921, PMID: 19234461

Moser M, Legate KR, Zent R, Fässler R. 2009b. The tail of integrins, talin, and kindlins. *Science* **324**:895–899. DOI: https://doi.org/10.1126/science.1163865, PMID: 19443776

Muzumdar MD, Tasic B, Miyamichi K, Li L, Luo L. 2007. A global double-fluorescent Cre reporter mouse. *Genesis* **45**:593–605. DOI: https://doi.org/10.1002/dvg.20335, PMID: 17868096

Potocnik AJ, Brakebusch C, Fässler R. 2000. Fetal and adult hematopoietic stem cells require beta1 integrin function for colonizing fetal liver, spleen, and bone marrow. *Immunity* **12**:653–663. DOI: https://doi.org/10.1016/S1074-7613(00)80216-2, PMID: 10894165

Prümmer O, Fliedner TM. 1986. The fetal liver as an alternative stem cell source for hemolymphopoietic reconstitution. *The International Journal of Cell Cloning* **4**:237–249. DOI: https://doi.org/10.1002/stem.5530040402, PMID: 2875117

Rossi FM, Corbel SY, Merzaban JS, Carlow DA, Gossens K, Duenas J, So L, Yi L, Ziltener HJ. 2005. Recruitment of adult thymic progenitors is regulated by P-selectin and its ligand PSGL-1. *Nature Immunology* **6**:626–634. DOI: https://doi.org/10.1038/ni1203, PMID: 15880112

Ruppert R, Moser M, Sperandio M, Rognoni E, Orban M, Liu WH, Schulz AS, Oostendorp RA, Massberg S, Fässler R. 2015. Kindlin-3-mediated integrin adhesion is dispensable for quiescent but essential for activated hematopoietic stem cells. *The Journal of Experimental Medicine* **212**:1415–1432. DOI: https://doi.org/10.1084/jem.20150269, PMID: 26282877

Scharffetter-Kochanek K, Lu H, Norman K, van Nood N, Munoz F, Grabbe S, McArthur M, Lorenzo I, Kaplan S, Ley K, Smith CW, Montgomery CA, Rich S, Beaudet AL. 1998. Spontaneous skin ulceration and defective T cell function in CD18 null mice. *The Journal of Experimental Medicine* **188**:119–131. DOI: https://doi.org/10.1084/jem.188.1.119, PMID: 9653089

Schmidt S, Nakchbandi I, Ruppert R, Kawelke N, Hess MW, Pfaller K, Jurdic P, Fässler R, Moser M. 2011. Kindlin-3-mediated signaling from multiple integrin classes is required for osteoclast-mediated bone resorption. *The Journal of Cell Biology* **192**:883–897. DOI: https://doi.org/10.1083/jcb.201007141, PMID: 21357746

Schmits R, Kündig TM, Baker DM, Shumaker G, Simard JJ, Duncan G, Wakeham A, Shahinian A, van der Heiden A, Bachmann MF, Ohashi PS, Mak TW, Hickstein DD. 1996. LFA-1-deficient mice show normal CTL responses to virus but fail to reject immunogenic tumor. *Journal of Experimental Medicine* **183**:1415–1426. DOI: https://doi.org/10.1084/jem.183.4.1415, PMID: 8666900

Scimone ML, Aifantis I, Apostolou I, von Boehmer H, von Andrian UH. 2006. A multistep adhesion cascade for lymphoid progenitor cell homing to the thymus. *PNAS* **103**:7006–7011. DOI: https://doi.org/10.1073/pnas.0602024103, PMID: 16641096

Shinkai Y, Rathbun G, Lam KP, Oltz EM, Stewart V, Mendelsohn M, Charron J, Datta M, Young F, Stall AM1992. RAG-2-deficient mice lack mature lymphocytes owing to inability to initiate V(D)J rearrangement. *Cell* **68**:855–867. DOI: https://doi.org/10.1016/0092-8674(92)90029-C, PMID: 1547487

Sligh JE, Ballantyne CM, Rich SS, Hawkins HK, Smith CW, Bradley A, Beaudet AL. 1993. Inflammatory and immune responses are impaired in mice deficient in intercellular adhesion molecule 1. *PNAS* **90**:8529–8533. DOI: https://doi.org/10.1073/pnas.90.18.8529, PMID: 8104338

Sperandio M, Pickard J, Unnikrishnan S, Acton ST, Ley K. 2006. Analysis of leukocyte rolling in vivo and in vitro. *Methods in enzymology* **416**:346–371. DOI: https://doi.org/10.1016/S0076-6879(06)16023-1, PMID: 17113878

Svensson L, Howarth K, McDowall A, Patzak I, Evans R, Ussar S, Moser M, Metin A, Fried M, Tomlinson I, Hogg N. 2009. Leukocyte adhesion deficiency-III is caused by mutations in KINDLIN3 affecting integrin activation. *Nature Medicine* **15**:306–312. DOI: https://doi.org/10.1038/nm.1931, PMID: 19234463

Tulunay O, Good RA, Yunis EJ. 1975. Protection of lethally irradiated mice with allogeneic fetal liver cells: influence of irradiation dose on immunologic reconstitution. *PNAS* **72**:4100–4104. DOI: https://doi.org/10.1073/pnas.72.10.4100, PMID: 673

Ueno T, Liu C, Nitta T, Takahama Y. 2005. Development of T-lymphocytes in mouse fetal Thymus organ culture. *Methods in Molecular Biology* **290**:117–133. PMID: 15361659

Ussar S, Wang HV, Linder S, Fässler R, Moser M. 2006. The Kindlins: subcellular localization and expression during murine development. *Experimental Cell Research* **312**:3142–3151. DOI: https://doi.org/10.1016/j.yexcr.2006.06.030, PMID: 16876785

Ussar S, Moser M, Widmaier M, Rognoni E, Harrer C, Genzel-Boroviczeny O, Fässler R. 2008. Loss of Kindlin-1 causes skin atrophy and lethal neonatal intestinal epithelial dysfunction. *PLoS Genetics* **4**:e1000289. DOI: https://doi.org/10.1371/journal.pgen.1000289, PMID: 19057668

Wagner N, Löhler J, Kunkel EJ, Ley K, Leung E, Krissansen G, Rajewsky K, Müller W. 1996. Critical role for beta7 integrins in formation of the gut-associated lymphoid tissue. *Nature* **382**:366–370. DOI: https://doi.org/10.1038/382366a0, PMID: 8684468

Weinstein EJ, Bourner M, Head R, Zakeri H, Bauer C, Mazzarella R. 2003. URP1: a member of a novel family of PH and FERM domain-containing membrane-associated proteins is significantly over-expressed in lung and colon carcinomas. *Biochimica et Biophysica Acta (BBA) - Molecular Basis of Disease* **1637**:207–216. DOI: https://doi.org/10.1016/S0925-4439(03)00035-8, PMID: 12697302

Wernimont SA, Wiemer AJ, Bennin DA, Monkley SJ, Ludwig T, Critchley DR, Huttenlocher A. 2011. Contact-dependent T cell activation and T cell stopping require talin1. *The Journal of Immunology* **187**:6256–6267. DOI: https://doi.org/10.4049/jimmunol.1102028, PMID: 22075696

Xu H, Gonzalo JA, St Pierre Y, Williams IR, Kupper TS, Cotran RS, Springer TA, Gutierrez-Ramos JC. 1994. Leukocytosis and resistance to septic shock in intercellular adhesion molecule 1-deficient mice. *Journal of Experimental Medicine* **180**:95–109. DOI: https://doi.org/10.1084/jem.180.1.95, PMID: 7911822

Ye F, Petrich BG, Anekal P, Lefort CT, Kasirer-Friede A, Shattil SJ, Ruppert R, Moser M, Fässler R, Ginsberg MH. 2013. The mechanism of kindlin-mediated activation of integrin αIIbβ3. *Current Biology* **23**:2288–2295. DOI: https://doi.org/10.1016/j.cub.2013.09.050, PMID: 24210614